UNIVERSITÉ DE MONTRÉAL

# INVESTIGATION OF THE FREQUENCY RESPONSE OF CONSTANT VOLTAGE ANEMOMETERS IN TURBULENT FLOWS

ATABAK SADEGHI HASSANLOUEI
DÉPARTEMENT DE GÉNIE MÉCANIQUE
ÉCOLE POLYTECHNIQUE DE MONTRÉAL

MÉMOIRE PRÉSENTÉ EN VUE DE L'OBTENTION
DU DIPLÔME DE MAÎTRISE ÈS SCIENCES APPLIQUÉES
(GÉNIE MÉCANIQUE)
JUIN 2014

© Atabak Sadeghi Hassanlouei, 2014.

UNIVERSITÉ DE MONTRÉAL

ÉCOLE POLYTECHNIQUE DE MONTRÉAL

Ce mémoire intitulé

INVESTIGATION OF THE FREQUENCY RESPONSE OF CONSTANT VOLTAGE ANEMOMETERS IN TURBULENT FLOWS

présenté par: SADEGHI HASSANLOUEI Atabak
en vue de l'obtention du diplôme de: Maîtrise ès sciences appliquées
a été dûment accepté par le jury constitué de:

Mme. ROSS Annie, Ph.D., présidente
M. VÉTEL Jérôme, Doct., membre et directeur de recherche
M. WEISS Julien, Ph.D., membre et codirecteur de recherche
M. LAURENDEAU Éric, Ph.D., membre

*This thesis is dedicated to my dear parents*

# Acknowledgment

It is my honour to express my best regards and deepest sense of gratitude to my advisor Prof. Jérôme Vétel for the continuous support of my study and research, particularly his patience, enthusiasm, motivation, and immense knowledge. I owe my success to his guidance and support throughout all the time of research and writing for this thesis. I would also like to thank my co-supervisor Prof. Julien Weiss for his guidance and support over the course of the research. Many thanks to my committee members Prof. Éric Laurendeau and Prof. Annie Ross for their suggestions that helped me improve quality of this thesis.

I express my deepest thanks to my family and friends for their enduring support throughout this process. I would like to express appreciation to my sisters Sanaz and Nouray and my dear friends MohammadHossein, Soroush, Shayesteh, Maryam, Meghan, Charlotte, Melissa, Masoud and Elham for always being a great supportive mentors and challenging my thoughts. Last but not least, a special thank goes to Justine for her endless support and motivation throughout this path.

# Résumé

Un prototype d'anémomètre disponible dans le commerce, l'anémomètre à voltage constant (CVA), est présenté et son principe de fonctionnement est étudié et analysé. Nous détaillons les différentes procédures et corrections qui doivent être appliquées aux signaux de tension afin d'obtenir les signaux de vitesse correspondant, et cela inclut l'inertie thermique du capteur. Les résultats sont comparés à un autre type d'anémomètre très répandu en recherche et dans l'industrie, l'anémomètre à température constante (CTA), à des fins de validation. Les mesures sont effectuées dans la région turbulente d'un jet turbulent axisymétrique, et incluent des vitesses moyennes, des écarts-types de fluctuations de vitesse et des densités spectrales d'énergie. Sur une même plage d'opération, nous montrons que les deux systèmes donnent des résultats similaires. Le CVA sous-estime légèrement les écarts-types de vitesse donnés par le CTA, ce qui est attribué a un effet non-linéaire. Nous montrons que la fréquence de coupure du CVA est plus élevée que le plus couramment utilisé CTA, et que le bruit électronique est plus faible. L'anémomètre à voltage constant offre donc une excellente alternative à l'anémomètre à température constante pour les écoulements faiblement turbulents dont le contenu fréquentiel est riche, comme les écoulements supersoniques et hypersoniques.

# Abstract

A commercially available anemometer system considered as a prototype, the constant voltage anemometer (CVA), is presented and its working principle is studied and analyzed. We detail the different procedures and corrections that have to be applied to voltage signals to deduce corresponding velocity signals, including the effect of the thermal inertia of the sensor. Results are compared to another anemometer system widely used in research and industry, the constant temperature anemometer (CTA), for validation requirements. Measurements are performed in the turbulent region of a subsonic axisymmetric jet and include mean velocities, root-mean-square (rms) values of velocity fluctuations and power spectral densities. In the same range of operation, we show that the two instruments give similar results. The CVA anemometer slightly underestimates the rms velocity values given by the CTA anemometer which is attributed to a non-linear effect. We show that the cut-off frequency of the CVA system is higher than the more commonly used CTA system, and that the electronic noise level is lower. The constant voltage anemometer is thus an excellent alternative to the constant temperature anemometer for low turbulent flows with rich frequency content, such as supersonic and hypersonic flows.

# Contents

Dedication . . . . . iii

Acknowledgment . . . . . iv

Résumé . . . . . v

Abstract . . . . . vi

Contents . . . . . vii

List of Tables . . . . . ix

List of Figures . . . . . x

List of Appendices . . . . . xii

List of Abbreviations and Acronyms . . . . . xiii

Chapter 1 Introduction . . . . . 1
- 1.1 General Objective . . . . . 2
- 1.2 Specific Objectives . . . . . 2
- 1.3 Thesis Structure . . . . . 2

Chapter 2 Literature review . . . . . 3
- 2.1 Basics of hot-wire anemometry . . . . . 3
- 2.2 Working principle . . . . . 5
- 2.3 The constant current anemometer . . . . . 8
- 2.4 The constant temperature anemometer . . . . . 8
- 2.5 The constant voltage anemometer . . . . . 10

Chapter 3 Experimental setup and measurement techniques . . . . . 13
- 3.1 Anemometer systems . . . . . 13
- 3.2 Acquisition systems . . . . . 13
- 3.3 Signal Processing . . . . . 14
- 3.4 The jet flow facility . . . . . 14
- 3.5 Flow field characterisation . . . . . 16
  - 3.5.1 Statistical convergence . . . . . 17

3.5.2 Exit velocity and turbulence profile . . . . . 19

Chapter 4 Constant voltage anemometer analysis . . . . . 21
4.1 Internal calibration of the CVA . . . . . 21
4.2 Measurement of the wire cold resistance . . . . . 23
4.3 Investigation of the wire termal inertia . . . . . 26
4.4 Compensation for the wire thermal inertia . . . . . 32
4.5 Results . . . . . 35

Chapter 5 Turbulent flow measurements . . . . . 42
5.1 Calibration procedure . . . . . 42
5.2 Mean and rms velocity profiles . . . . . 46
5.3 Turbulent spectra . . . . . 49
5.4 Velocity profiles . . . . . 50

Chapter 6 Conclusion . . . . . 55

Bibliography . . . . . 58

Appendices . . . . . 62

# List of Tables


3.1 Summary of experimental setup . . . . . 17

4.1 Values of coefficients $a$ and $b$ for CVA systems . . . . . 23

4.2 TC values obtained from the measurements compared with the manufacturer data. . . . . 36

5.1 Influence of the software correction on the mean velocity values (m/s). 53

5.2 Influence of the software correction on the rms velocity values (m/s). 53

# List of Figures


2.1 Exemple of velocity time signal recorded at 4096 Hz in a turbulent flow. 4
2.2 Typical wire sensor used to measure turbulent flows. . . . . 4
2.3 Example of a hot-wire system. . . . . 5
2.4 Energy balance of a heated wire. . . . . 6
2.5 Electronic circuit of the CCA anemometer. . . . . 9
2.6 The circuit of a typical CTA anemometer. . . . . 9
2.7 Electronic circuit of the CVA anemometer ($R_w$: sensing wire). . . . . 11
3.1 The jet flow facility (not in scale). . . . . 14
3.2 Axisymmetric nozzle section . . . . . 16
3.3 Convergence of mean and rms values at $r/R = 0$ (green line) and at $r/R = 1$ (blue line). . . . . 18
3.4 Radial turbulent profiles at the jet exit section ($x/D < 0.1$). . . . . 20
4.1 Electronic circuit of the CVA anemometer ($R_w$: sensing wire). . . . . 22
4.2 CVA Internal Calibration . . . . . 22
4.3 CVA, wire cold resistance estimation . . . . . 25
4.4 Sample of several responses (colored lines) to the square wave test as well as the phase-averaged response (black line). Note that one point over 4 is presented in the phase averaged response . . . . . 29
4.5 Sample of a wire response to square wave test. Inset: Closer look at the same graph, $M_{\mathrm{CVA}}$ is the time from maximum untill 63 % drop in the voltage (in this example it is $\simeq 3.2 \times 10^{-4}$ s) . . . . . 30
4.6 Convergence of the $M_{\mathrm{CVA}}$time constant with the number of averages. 31
4.7 Evolution of $M_{\mathrm{CVA}}$ as in equation (4.10). Dashed line shows the nominal value . . . . . 31
4.8 CVA anemometer circuits. . . . . 33
4.9 Sine wave test setup . . . . . 36
4.10 Bode plot for the CVA 1, for both TC1 (point "a") and TC2 (point "b") settings, with the constant 3 dB line plotted in grey for reference. The inclined line has 20dB/dec slope. . . . . 39
4.11 Detailed views of figure 4.10. . . . . 39
4.12 Bode plot for the CVA 2, for both TC1 (point "a") and TC2 (point "b") settings, with the constant 3 dB line plotted in grey for reference. The inclined line has 20dB/dec slope. . . . . 40
4.13 Detailed views of figure 4.12. . . . . 40

4.14 Power spectral density of voltages from CH1 and TCM outputs of same instrument. Inset: Closer look at the high frequency zone . . . . . 41
5.1 Positioning of the pitot-static tube and the hot-wire during the calibration procedure. . . . . 43
5.2 Thermal boundary layer developing on the wire. . . . . 44
5.3 Examples of two different calibration curves. . . . . 46
5.4 Test on the repeatability of the calibration procedure. . . . . 46
5.5 Zones of turbulent axisymmetric jet . . . . . 47
5.6 Radial turbulent profiles at $x/D = 12$. . . . . 49
5.7 Power spectra of velocity fluctuations at $x/D = 12$. . . . . 51
5.8 Radial turbulent profiles at $x/D = 12$ . . . . . 52
5.9 Turbulent intensity profiles at $x/D = 12$ . . . . . 52
A.1 Electronic circuit of the CVA anemometer ($R_w$: sensing wire). . . . . 63
B.2 The circuit of the CTA anemometer with the square wave injection . 66
B.3 Response of the MiniCTA anemometer to a step signal. . . . . 66
B.4 Transfer function of the MiniCTA anemometer deduced from the square wave test. . . . . 67
B.5 Response of the MiniCTA anemometer to a 80 mV step signal. . . . . 69
B.6 Example of an ideal response of a well-adjusted CTA system to a square-wave test (adapted from Freymuth (1967); Bruun (1995)). . . 70
B.7 The analyzing of the DISA CTA transfer function . . . . . 71
B.8 Comparision of Fourier transform of step response for both types of CTA systems (Figures B.7b and B.4), higher frequency bandwidh and smaller gain for DISA system can be seen here . . . . . 71
C.9 Power spectra of velocity fluctuations measured on the jet axis at $x/D = 12$ for $Re \simeq 160\ 000$. . . . . 72

# List of Appendices

Appendix A: Governing equations of CVA . . . . . 62

Appendix B: The frequency response of the constant temperature anemometer . . . 64

Appendix C: Example of complete hardware compensation . . . . . 72

# List of Abbreviations and Acronyms

## Acronyms

| | |
|---|---|
| CTA | Constant Temperature Anemometer |
| CVA | Constant Voltage Anemometer |
| CCA | Constant Current Anemometer |
| CFM | Cubic Feet per Minute |
| RC | Resistor Capacitor |
| RPM | Revolutions Per Minute |
| PSI | Pounds per Square Inch |
| DAQ | Data Acquisition |
| TCM | Time Constant Measurement |
| PDR | Power Dissipation Ratio |
| TC | Time Constant |

## Usual Characters

| | |
|---|---|
| $E$ | Energy (J) |
| $W$ | Work (J) |
| $Q$ | Heat (J) |
| $R$ | Resistance ($\Omega$) or Radius of the nozzle output (m) |
| $I$ | Electrical current (A) |
| $h$ | Heat transfer coefficient (W/m$^2$K) |
| $T$ | Temperature (K) or (℃) |
| $Nu$ | Nusselt number |
| $m$ | Mass (Kg) |
| $c$ | Specific heat capacity (Kj/KgK) |
| $U$ | Velocity (m/s) |
| $V$ | Voltage (V) |
| $Re$ | Reynolds number |
| $D$ | Diameter of the jet flow when exiting the nozzle (m) |
| $l$ | length of the sensing wire (m) |
| $d$ | Diameter of the sensing wire (m) |

| | |
|---|---|
| $x$ | Axial distancing (m) |
| $r$ | Radial distancing (m), Resistance fluctuations ($\Omega$) |
| $r_L$ | Lead Resistance ($\Omega$) |
| $f$ | Frequency (Hz) |
| $C$ | Capacitance (F) |
| $j$ | $\sqrt{-1}$ |
| $P$ | Pressure (Pa) |

**Greek Letters**

| | |
|---|---|
| $\chi$ | Temperature coefficient ($K^{-1}$) |
| $\kappa$ | Thermal conductivity (W/mK) |
| $\alpha$ | Overheat ratio |
| $\rho$ | Density ($Kg/m^3$) |
| $\mu$ | Dynamic viscosity (Pa s) |
| $\omega$ | Angular frequency (Hz) |

**Symbols**

| | |
|---|---|
| $\dot{(\ )}$ | Temporal rate |
| $\frac{d(\ )}{dt}$ | Temporal derivation |
| $(\ )_w$ | Characteristics at heated wire or based on wire diameter |
| $(\ )_a$ | Characteristics at ambient condition |
| $(\ )_f$ | Characteristics at film temperature |
| $\overline{(\ )}$ | Mean temporal value |
| $(\ )'$ | Fluctuating values such as $\overline{(\ )'} = 0$ |

**Special Characters**

| | |
|---|---|
| $\mathscr{F}$ | operator of the Fourier transform |

# Chapter 1
# Introduction

In fluid mechanics, the thermal anemometry is one of the oldest anemometry technique used to capture instantaneous point-wise velocity in gas and liquid flows. Although other more recent techniques have emerged since, the thermal anemometry remains the most accurate technique due to its very fine spatial resolution and high-frequency response, thus outperforming any other technique. The working principle is based on a heated wire, placed in a fluid, that is cooled by the flow, whose local velocity is deduced from a calibration function. Since in turbulent flows, where a large number of time scales can coexist, the spectral content of velocity time fluctuations is of primary importance, this so-called hot-wire technique is widely used in research laboratories as well as in industry, particularly in wind-tunnels for aerodynamics studies.

Three types of thermal anemometers are currently available. The constant current anemometer (CCA) is historically the first thermal anemometry system, however it is not used in velocity measurements any-more. The most used technique is the constant temperature anemometer (CTA), where the wire is maintained at a prescribed temperature, which also means that its resistance is constant. Afeed-back loop, feeds the wire with the adequate current (to keep its temperature constant) and provides an output signal. We work with the output signal to deduce the velocity. The CTA system is adapted to most applications, from research to engineering problems, but is limited for specific problems, as in supersonic, and more so in hypersonic turbulent flows where velocity fluctuations can exceed several megahertz. To obtain a frequency response better than the CTA system, the constant voltage anemometer (CVA) has been introduced, which keeps the wire voltage constant instead of its resistance. However, contrary to the CTA system that is a very common tool for the scientific community, the CVA system is much less known, to such an extent that even some CTA users have never heard about this technique.

The reasons for this lack of knowledge surely come from the fact that the CTA system generally suffices to most problems, and that only one company all around the world manufactures CVA anemometers. However, the advantage of the CVA over the CTA is not limited to the frequency response. Indeed, it is less sensitive to electromagnetic, radio-frequency interferences and connectivity effects. Which explains why such systems are used by NASA and the US Air Force. Furthermore, a CVA anemometer is also less expensive that a CTA system presenting the same performances.

## 1.1 General Objective

Despite the introduction of the CVA anemometer 20 years ago it is can still at best be considered a prototype and is not well understood or commonly used today. A robust procedure to perform accurate CVA measurements is still lacking, and CVA signals have never been compared to another technique to analyze its frequency response. The primary objective of this study is to conduct a robust CVA measurement in turbulent flow, comparing it with CTA anemometer.

## 1.2 Specific Objectives

The circuit and operation of a commercially available constant voltage anemometer needs to be described. The wire introduces a time lag (time constant) which varies with the velocity and needs to be measured and calibrated. The wire response needs to be corrected through a software compensation that can be performed either in the temporal domain or in the frequency space. The CTA anemometer needs to be analysed by measuring its frequency response since it is the reference system. A reliable calibration procedure will relate the anemometers output voltage to velocity, and finally the velocity data would be compared with each other. What we expect is that one physical phenomenon recorded by two different systems will be represented in the same manner.

## 1.3 Thesis Structure

The manuscript is organized as follows. We first begin introducing state of the art anemometer systems, by presenting the numerous working principles and listing the main advantages and drawbacks of each system (chapter 2). Then the different anemometers used in the framework of this study are presented in chapter 3 followed by the flow facility chosen to generate reference velocity signals. The operation of a CVA is then dissected in chapter 4 and in chapter 5 we show that some precautions must be taken while using CTA output as the the reference signals. Results are presented in chapter 6. In this latter chapter, CTA and CVA velocity signals are compared in terms of mean and rms values, as well as power spectral densities.

# Chapter 2
# Literature review

This section covers the basics of hot-wire anemometry. The working principles of the different existing systems are briefly explained as well as their advantages and disadvantages, and some examples of their applications in industry and in science are given.

## 2.1 Basics of hot-wire anemometry

Three main techniques are commonly used to measure the local velocity in a flow. Optical-based techniques such as the Laser Doppler and the particle image velocimetry are the most recent techniques and also the most attractive since they are not intrusive and quite easy to use, despite requiring lasers and complex optics. On the other hand the oldest technique, hot-wire anemometry, is still a widely used technique and remains the most accurate one for turbulent flow temperature and velocity measurements. The reasons come from the very high frequency response of hot-wire anemometers (up to hundreds of kilohertz), the wide velocity range that can be covered (from subsonic to supersonic), the relative low cost compared to other techniques, the high signal to noise ratio, the ease to process signals (the output is an analogue voltage), and the existence of various commercially available probes and anemometers. Even if the technique is intrusive, the flow disturbance is minimal due to a good spatial resolution since the sensor is very small. With multi-sensor probes it is possible to simultaneously measure the temperature and two or three components of the velocity vector (and even the vorticity for most complex sensors). An example of a velocity signal recorded by a hot-wire anemometer is presented in figure 2.1.

The working principle of hot-wire systems is to maintain a very fine sensor, the wire, at a temperature much higher than the flow to study, and to derive the local velocity from the heat exchange between the sensing element and the fluid. As a consequence, the technique requires a calibration that is not always easy to obtain depending on the flow considered, and which has to be regularly renewed since it depends on numerous parameters, as the ambient temperature, pressure and humidity, or the ageing of the wire. It is for this reason that the hot-wire technique is not always preferred or is used in the wrong way. On the other hand, the accurate measurement of a complex turbulent signal cannot be simply obtained. If, on the contrary, the technique is perfectly mastered, then numerous informations can be obtained on the flow, including mean and rms values, skewness and flatness coefficients, power spectral density, etc.

Based on the probe type, one or several sensing wires with different orientations and

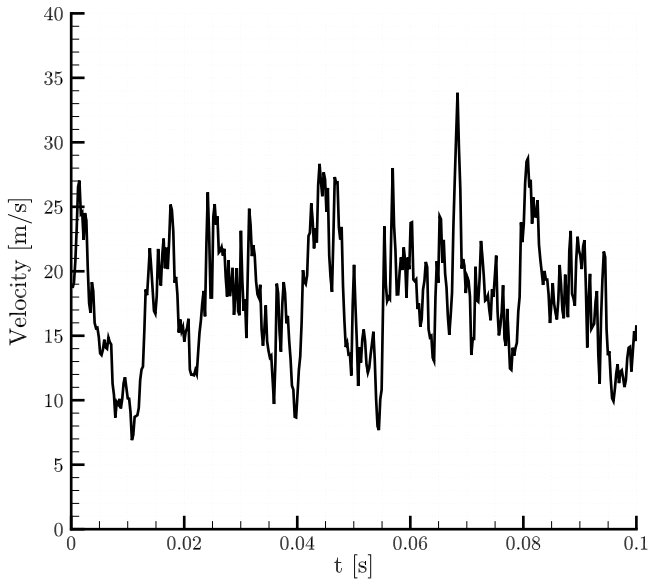


Figure 2.1: Exemple of velocity time signal recorded at 4096 Hz in a turbulent flow.

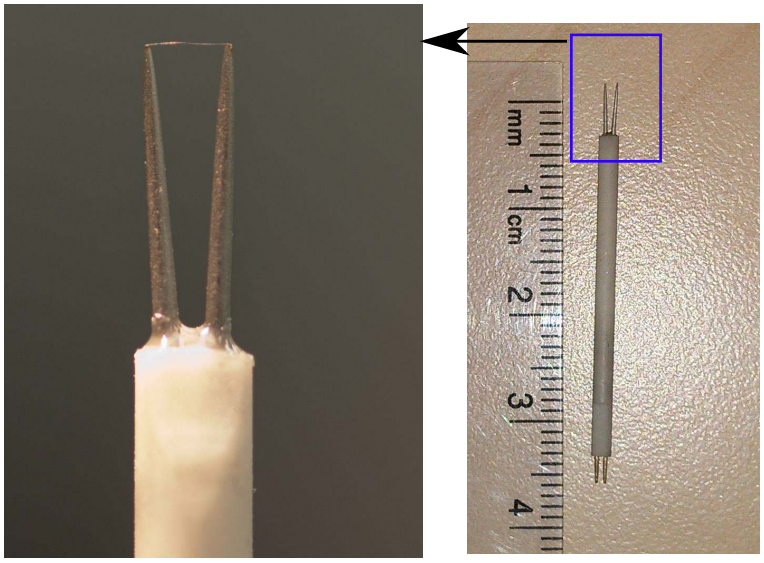


Figure 2.2: Typical wire sensor used to measure turbulent flows.

materials can be used. A typical single sensor probe is shown in figure 2.2 and a full hot-wire system diagram in figure 2.3. The sensing wire, generally made in tungsten, is welded between two metallic needle-shaped prongs and is placed perpendicular to the main flow direction.

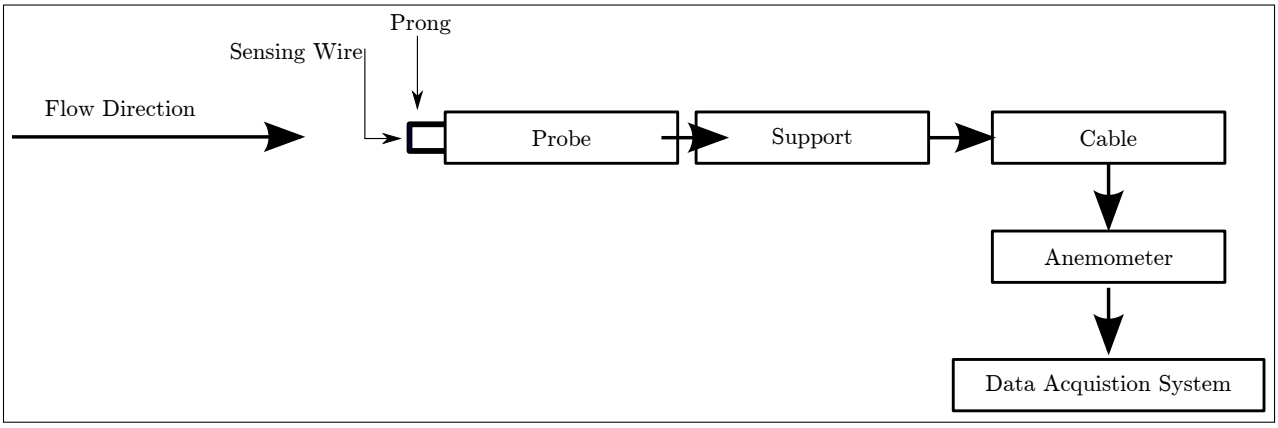


Figure 2.3: Example of a hot-wire system.

The sensor is inserted in a probe support connected to the anemometer that delivers a voltage signal that can be recorded by a standard acquisition card.

## 2.2 Working principle

The hot-wire anemometry relies on the wire temperature changes due to the heat transfer between the heated wire and the flow, which can also lead to changes of the wire resistance. The circuits used at hot-wire anemometers can vary from one system to the other but basically the measurable output voltage is related to the energy that is required to keep the wire hotter than the measured flow. For the sensor used in our experiments, the length is 1.25 mm for a diameter of 5µm giving an aspect ratio of 250, and thus the hot-wire sensor can be theoretically considered as an infinite cylinder (Hultmark and Smits, 2010). Regardless of the anemometer used, the conservation of energy for a wire element as schematically shown in figure 2.4 can be written in the following form:

$$\frac{dE}{dt} = \dot{W} - \dot{Q}, \tag{2.1}$$

*i.e.* the change of energy (dE/dt) is a balance between the rate of work done by the wire ($\dot{W}$) and the heat exchange with the ambient fluid ($\dot{Q}$).

The work term in equation 2.1 corresponds to the Joule heating of the wire and can be expressed as $\dot{W} = R_w I_w^2$ which depends on the wire resistance $R_w$ and the current $I_w$ passing through the wire. If we assume that the heat conduction from the wire to the supporting prongs is negligible, then $Q$ represents the energy transfer between the wire and the flow, and is a heat loss since the wire is always kept at a higher temperature than the flow. $Q$ is the

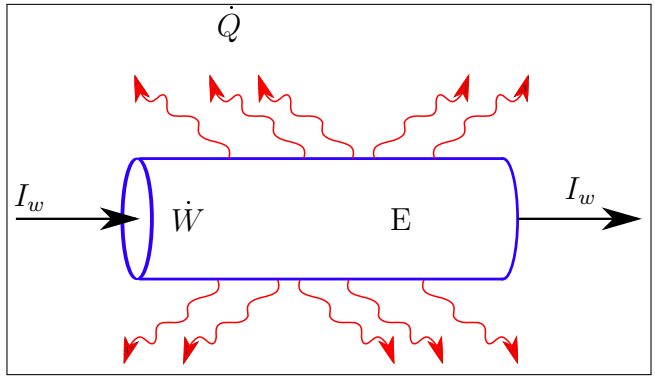


Figure 2.4: Energy balance of a heated wire.

sum of conduction and convection losses. Radiative heat transfer has indeed been estimated to be about $10^{-4}$ times the heat received by the wire (Comte-Bellot, 1976) and therefore is assumed to be negligible. Finally, for a 5µm conventional wire used in velocities above 0.1 m/s free convection effects can be neglected so that only forced convection need to be considered (Hultmark and Smits, 2010).

Since the wire is very small, we suppose that the heat transfer between the wire and the flow is homogeneous, and that the temperature distribution is uniform along the wire length. Therefore, the convective heat flux between the wire and the fluid can be written with Newton's law:

$$\dot{Q} = hA(T_w - T_a) = \pi dlh(T_w - T_a) \tag{2.2}$$

in which $A$ is wire cross-section area, $l$ and $d$ are the wire length and diameter, $T_w$ is the wire temperature, $T_a$ is the ambient temperature and $h$ is the heat transfer coefficient (W/m$^2$K). The non-dimensional Nusselt number is the ratio of convective to conductive heat transfer and is defined as:

$$Nu = \frac{hd}{\kappa} \tag{2.3}$$

in which $\kappa$ is the thermal conductivity of the flow (W/m K). If the wire has a mass $m_w$ and a specific heat capacity $c_w$, the energy can be related to the wire temperature through:

$$\frac{dE}{dt} = m_w c_w \frac{dT_w}{dt} \tag{2.4}$$

By inserting the Nusselt number definition and equations 2.2 and 2.4 in equation 2.1, we finally obtain:

$$m_w c_w \frac{dT_w}{dt} = R_w I_w^2 - \pi l \kappa (T_w - T_a) Nu, \tag{2.5}$$

which relates the electric current and the wire resistance to the flow parameters. Here, the time derivative of the wire temperature appears as a thermal inertia term. The flow velocity $U$ is not directly apparent in this relation but is in fact included in the Nusselt number. The detail of the relation $Nu = f(U)$ will be further explained in section 5.1.

Knowing the physical characteristics of the metal with which the wire is made, its resistance is assumed to be a function of only the temperature through the wire temperature coefficient $\chi$:

$$R_w = R_a[1 + \chi(T_w - T_a)] \tag{2.6}$$

where $R_w$ and $R_a$ are the wire resistances at wire temperatures $T_w$ and $T_a$, respectively. The heating of the wire is quantified by the overheat ratio defined by

$$\alpha_w = \frac{R_w - R_a}{R_a}. \tag{2.7}$$

As the hot-wire resistance changes with both temperature and velocity, for low overheat ratios the wire is more sensitive to temperature fluctuations (behaves mostly as a thermometer, and besides the technique is called cold-wire) and for higher overheat ratios it is more sensitive to velocity fluctuations (behaves mostly as an anemometer). The maximum limit of the overheat ratio is chosen based on the wire material and the fluid medium. In water for example, it is not possible to reach a high value because the heat exchange with a liquid is higher than with a gas which means it is more difficult to maintain a high wire temperature. Also when the wire is heated to high temperatures, bubbles form around the wire which effect the heat transfer notably. For these reasons maximum overheat ratio for liquids is in the order of 0.1. In air, which is the fluid used in this study, the overheat ratio (*i.e.* the wire temperature) can be arbitrarily high, but in practice, a high value can lead to wire oxidization, deformation or burn out. The overheat ratio is thus usually chosen between 0.5 to 1.

It is preferred that the temperature coefficient $\chi$ be high because any small temperature change results in a measurably large resistance change. For example, the tungsten's resistance doubles with respect to its resistance in room temperature, when heated at 250 K. The wire conducting metal should also resist to high temperatures and should be sufficiently resistant to preserve its shape whatever the flow velocity. Some commonly used metals are tungsten, platinum, platinum-rhodium alloy or platinum-iridium alloy.

The key point in hot-wire anemometry is the thermal inertia of the wire. Indeed, we want to deduce the velocity from the heat transfer between a heated wire and a medium, however the wire response is not ideal. Basically, the transfer function can be viewed as a first order system, which means that the wire sensitivity decreases as the velocity frequency increases above a characteristic cut-off frequency. From this observation, three types of

anemometers will now be briefly described, the constant current anemometer (CCA), the constant temperature anemometer (CTA) and the constant voltage anemometer (CVA).

## 2.3 The constant current anemometer

The CCA anemometer was used as early as 1920s to study wind velocity and direction and represented a major step forward compared to wind vanes used before. It is historically the first system to use a hot-wire to measure flow velocity. The basic constant current anemometer circuit is shown in figure 2.5. It consists of a Wheatstone bridge and a RC amplifier circuit. The bridge permits the adjustment of the wire heating and the amplifier (ultra-low noise and high gain) amplifies the output signal helping to compensate for the wire thermal lag. The bridge is balanced (checked with the galvanometer G) by adjusting the resistances $R_s$ and $R_3$, and the corresponding current $I_w$ is measured by the ammeter A. With the RC compensating circuit the frequency response of a CCA system can reach up to 300 kHz as reported by McKeon *et al.* (2007) and Comte-Bellot (1976). However, when the flow has moderate fluctuations (turbulence level larger than 5%, Comte-Bellot, 1976), harmonics of circuit are generated by parametric excitation and even amplified by the RC circuit (McKeon *et al.*, 2007). Due to these strong non-linearities this system is almost no longer used today. The circuit is however still used with a cold wire to measure fluctuating temperature in oscillating flows (Berson *et al.*, 2010a,b) and more generally in turbulence.

## 2.4 The constant temperature anemometer

One way to circumvent the drawbacks of the CCA system is to weaken the effect of the wire thermal lag. To achieve this the best method is to keep the wire operational temperature constant, *i.e.* the resistance is constant, and equation 2.5 becomes:

$$R_w I_w^2 = \pi l \kappa (T_w - T_a) Nu. \tag{2.8}$$

It was known since 1940s that a rapid compensation to flow fluctuations can be achieved using a feedback circuit. Thus the constant temperature anemometer (CTA) was introduced and became common usage in the 1960s, and is still the most commonly used thermal anemometry system nowadays. The circuit of a typical CTA anemometer is shown in figure 2.6.

The circuit is mainly composed of a Wheatstone bridge and a feedback amplifier. By adjusting the resistance $R_3$ of the bridge, the wire resistance can be set to any desired value so that its temperature can be adjusted to the desired value (usually between 200 and 300°C).

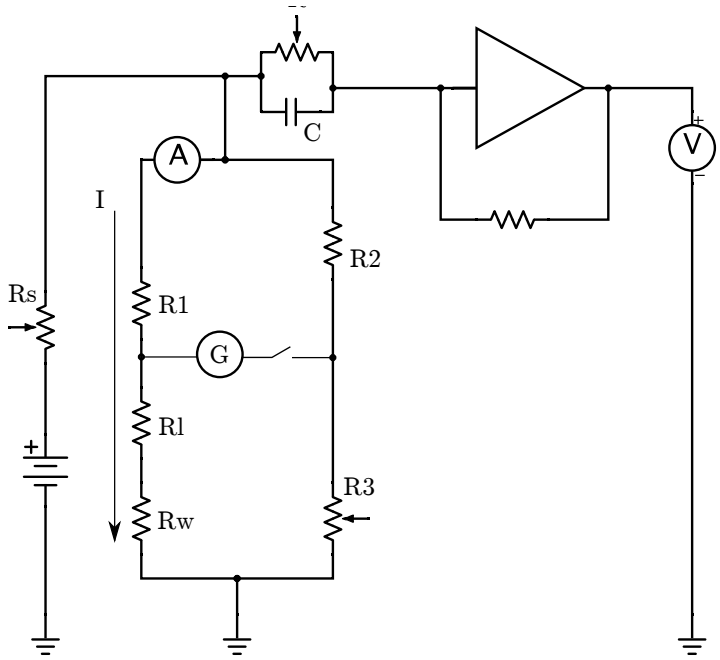


Figure 2.5: Electronic circuit of the CCA anemometer.

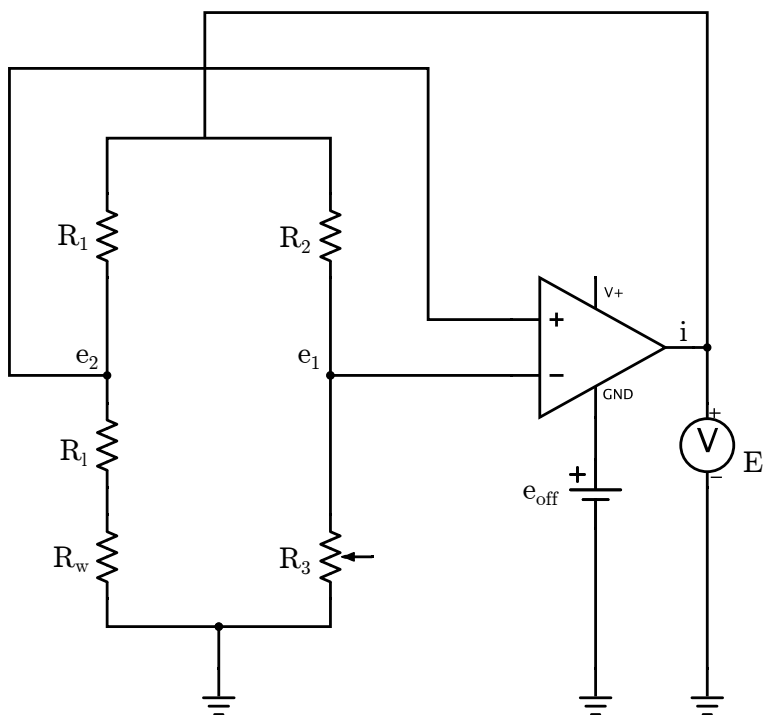


Figure 2.6: The circuit of a typical CTA anemometer.

$T_w$ can be obtained from equation 2.6

$$T_w = T_a + \left(\frac{R_w}{R_a} - 1\right)\frac{1}{\chi}.$$

In practice, the wire operating temperature is chosen based on some limitations (wire oxidization, deformation, etc.) which has been explained in section 2.2.

Any change in the flow velocity and temperature leads to a change in the wire resistance which leads to a voltage difference between the two sides of the bridge, namely nodes $e_1$ and $e_2$. This voltage difference is fed to the amplifier, and the output current $i$ delivered by the amplifier is proportional to the resistance change of the sensitive wire. Thus the frequency response of the CTA depends on how fast the feedback differential amplifier can return the current $i$ to the top of the bridge to return the wire resistance to its initially selected value.

Contrary to CCA systems, CTA systems are much less sensitive to non-linearities for moderate to even large flow fluctuations, in particular if the cut-off frequency of the system is finely tuned to be ten times the frequencies of largest amplitude fluctuations (Bruun, 1995). However, while theoretically the maximum frequency response of a CTA system should be in the order of 400 kHz, which is also the frequency advanced by commercial manufacturers, in practice it is limited by $\sim$ 100 kHz (McKeon *et al.*, 2007), a limit that can be increased up to 300 kHz by post-processing the data and applying additional signal corrections, as shown in a Mach 2.5 supersonic flow by Weiss *et al.* (2001). However, this frequency is velocity dependent, and is still not sufficient to study most supersonic and hypersonic flows where turbulent fluctuations can reach several MHz. Another drawback of the CTA system is that its sensitivity to velocity and temperature is highly dependent on the cable capacitance and inductance, and if the bridge is unbalanced, the sensitivity can be even lower.

## 2.5 The constant voltage anemometer

The third type of anemometer consists in keeping not the intensity, nor the resistance, but the voltage through the wire ($V_w = R_w I_w$) constant independently of the wire resistance. The heat transfer between the wire and the flow changes the wire resistance, which means that the overheat ratio is not constant and depends on the local velocity contrary to the CTA system, which leads also to a change in the passing current $I_w$. The idea and first realization of such a circuit, presented in figure 2.7, was introduced by Sarma (1991). $I_w$ is passed through a large resistance $R_a + R_b$ and the anemometer output $V_s$ is closely related to the voltage changes across $R_a + R_b$. The CVA output voltage is larger by a factor of 20 compared to CCA and a factor of 2 compared to CTA (McKeon *et al.*, 2007). A secondary

resistor $R_d$ is used to limit this output and to keep it in the range of most acquisition systems. As for the CCA anemometer, the CVA system includes a RC operational amplifier circuit to compensate for the wire thermal lag (term $dT_w/dt$ in equation 2.5). This circuit and the thermal lag compensation are one of the main focuses of the present research and will be further analyzed in upcoming chapters.

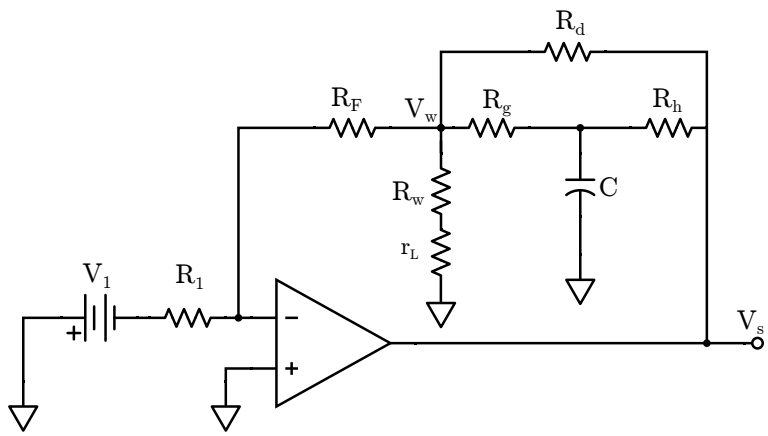


Figure 2.7: Electronic circuit of the CVA anemometer ($R_w$: sensing wire).

The CVA system has the highest frequency response ($\sim$ 600 kHz) among all available anemometers. Sarma (1998) conducted several tests on two prototypes with nominal bandwidths of 15 and 350 kHz and showed that the bandwidth of the CVA did not change with the Reynolds number (from 8.7 to 17.3 based on a wire of 5 μm in diameter) or the wire overheat ratio (form 1.12 to 1.6). Comte-Bellot *et al.* (2004) showed that the CVA system response is slightly related to lead (cable) resistance (shown by $r_L$ in figure 2.7), however the effect of lead resistance on the time constant and sensitivity coefficients almost cancel each other so that the lead resistance effect can be omitted in calculations (McKeon *et al.*, 2007). There is no limitations in the capacitance and inductance of the cables in the CVA anemometry and no noise is added by extending cable length, in contrast to the other two anemometer types. When the wire is exposed to large velocity fluctuations, electronic harmonics are generated as for the CCA system. However, contrary to the CCA system, these unwanted harmonics can be removed for the CVA using a post-processing treatment (Berson *et al.*, 2009).

The CVA anemometer therefore offers several advantages over the other systems, and is the single system adapted to supersonic flows. It is also less expensive than most advanced CTA systems. The CVA is also far more than a laboratory tool and can be used in engineering applications as well. For example, Mangalam (2004) used an array of hot films operated with miniaturized CVA anemometers to capture the instantaneous shear stress distribution on a NACA0012 airfoil. The full device was placed on a F-15 aircraft where the tests were

performed and found that the CVA is immunized to electromagnetic interference (EMI), radio-frequency interference (RFI), temperature drift and cable capacitance effects. The high frequency bandwidth of the CVA caught the attention of many researches working in supersonic and hypersonic fluid dynamics where high frequency contents are crucial in the phenomena investigated. Comte-Bellot and Sarma (2001) applied different methods of thermal lag compensation in a Mach 2.3 flow. Kegerise and Spina (2000) compared the sensitivity of the CVA and the CTA, while Weiss *et al.* (2005) compared the spectra of CTA and CVA in a turbulent boundary layer at Mach 2.5 and concluded that the results of both systems after conducting software corrections are in good agreement when the signal to noise ratio is above one for both systems, which meant up to 200 kHz for their systems. Several studies have also been done in the transition region of a hypersonic boundary layer at NASA Barre *et al.* (1992); Blanchard *et al.* (1997). Last but not least, the CVA has also been used in hydrodynamics for detecting the boundary layer transition on the body of a boat as reported by Sarma *et al.* (1998).

Bandwidth of the CVA system depends on the RC operational amplifier circuit. For this reason the amplifier is chosen to achieve high frequency response and is not always capable of fully compensating the wire thermal lag. A complete compensation is done later using data processing, called software correction. This two-step procedure ensures a constant frequency bandwidth regardless of flow and wire conditions. In spite of the fact that CVA system has been introduced two decades ago, no successful comparison of CVA and CTA measurements have been conducted and to date these two systems have not been compared in spectral and time domain. For this reason this research will focus on comparing measurements done using both systems in incompressible turbulent flow, assuming CTA system as a reference system.

# Chapter 3
# Experimental setup and measurement techniques

The high frequency response of CVA anemometers is one of the main advantages of these system compared to CTA and CCA anemometers. For this reason, to study the CVA system, a flow with a developed turbulence zone with a high frequency content and moderate fluctuations had to be chosen, preferably without flow reversal zones. An air flow discharging through a circular axisymmetric nozzle into a stagnant air environment was chosen due to its simple geometry and the existence of a vast literature on the topic. Before presenting the flow facility, a review of measurement techniques available in our laboratory is given.

## 3.1 Anemometer systems

The CVA system that we have studied is a 4-channel model 4-600 CVA manufactured by *TAO SYSTEMS*. The 4 parallel channels were designed to permit using different sensors simultaneously. Each channel has two outputs. One is the raw, non-filtered signal, the other is the same signal low-passed filtered at a frequency chosen between 1 to 512 kHz. Filtered outputs deliver a voltage in the range $\pm 10$ V while non-filtered outputs deliver a voltage in the range 0-20 V. The system has a partial compensation setting for the wire time lag that will be discussed in the following chapter, and also a secondary circuit that allows the measurement of this time lag.

The CVA velocity signals were compared to CTA signals and several anemometers of this type were at our disposal, the DANTEC Dynamics multichannel MiniCTA 54N80 and the DISA 55M10 system. Additional details will be provided in section 6 but the main differences between the two systems is that according to the manufacturer, the former has a bridge ratio of 1:20 that cannot be adjusted, with a maximum probe current of 230 mA and a maximum frequency response of $\sim$ 10 kHz for conventional probes, whereas the latter is equipped with potentiometers to adjust the bridge to the desired value. We will also see in the following chapters the effect of these particularities on the results.

## 3.2 Acquisition systems

All anemometer output voltages (and pressure data) were recorded by National Instruments PXI-4495 24-Bit data acquisition systems with a maximum acquisition frequency of 204 800 Hz. The measurement of the wire thermal lag required higher frequencies and was

measured with a National Instruments PXI-5922 24-Bit Flexible-Resolution Digitizer that can reach a sampling rate of 15 MHz. All cards have their own anti-aliasing filters, which are on-board low-pass filters that remove the frequency content higher than $\sim 0.48$ times the acquisition frequency, *i.e.* a little bit lower than the Nyquist frequency. The cards were installed on the National Instruments PXI-8109 Embedded Controller to minimize the noise sources.

## 3.3 Signal Processing

For spectral analysis, raw data was divided in blocks on which a Hanning window function was applied. The blocks had 0% overlap. The choice for this window is that it is conventionally used in turbulence studies. The Fourier transform of each block was then computed and averaged over all blocks to provide the power spectral density. The number of samples per block was chosen according to the desired frequency resolution or the desired level of convergence of the computed spectrum. Signals presented in this study are generally recorded at 204 800 Hz for 30 s, and spectra are obtained from 187 averaging of blocks of 32 768 points, unless otherwise stated.

## 3.4 The jet flow facility

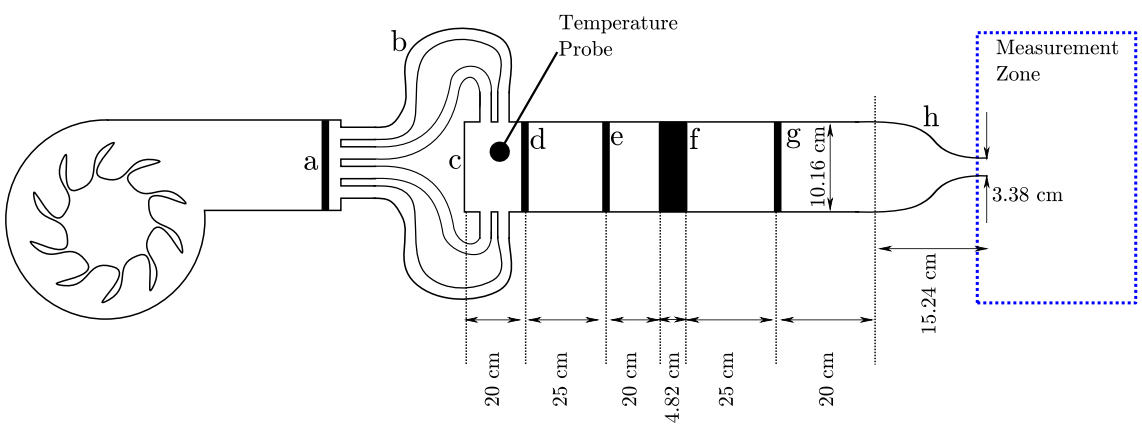


Figure 3.1: The jet flow facility (not in scale).

The flow facility is schematically presented in figure 3.1. An industrial air blower (*cincinnati fan* model HP-4C22) able to provide up to 100 CFM at static gauge pressure of 35 inches of water at room temperature was chosen. The blower had 10 blades which were rotated by

a 60 Hz engine with a maximum rotation speed of 3500 RPM. The engine was controlled from a computer through a National Instruments PXI-6229 (16-Bit) through a *SIEMENS Sinamics G110* frequency inverter and a controller allowing us to maintain the desired RPM of the fan, keeping the flow-rate constant.

Airflow was passed through a filter (marked with "a" in the figure) to remove dust and external particles, then through four high pressure (200 PSI) hoses (marked with "b" in the figure) to deliver air into the injection module from four sides. The hoses were chosen instead of a long straight pipe to break the geometry thus to prevent acoustic resonance in the flow. The four pipes were connected to the injection module from four sides, leaving the back of the module (marked with "c" in the figure) free to install an external flow excitement system for future usages. In this experiment the back side of the module was closed.

The injection module was designed to reduce the turbulence level of the flow, and to obtain a uniform velocity at the jet exit section. To this end, a set of one honeycomb, two different wire screens and a nozzle composes the injection module. This module reduces lateral and radial components of the mean flow velocity as much as possible. The dimensions of the components was carefully selected after a detailed review of the existing literature, and mainly from Hancock and Johnson (1997); Scheiman and Brooks (1981); Mikhailova *et al.* (1994); Tan-Atichat *et al.* (1982). After installing every component the axial turbulence intensity profile inside the module was obtained. Using this profile the distancing of next component was determined as the location of lowest turbulence level. The final set-up was designed with this step-by-step method. A perforated plate (marked with "d" in the figure) was used to trigger mixing of the flow which came from the four pipes. A steel wire cloth screen with 1.60 mm wire diameter and 56% open area ratio was used as a coarse screen (marked with "e" in the figure). A honeycomb with a length to diameter ratio of 14.5 was chosen to remove the radial component of the velocity providing a dominantly axial flow (marked with "f" in the figure). A galvanized steel wire cloth with 0.508 mm wire diameter and 57% open area ratio screen was used downstream as a fine screen (marked with "g" in the figure). The distances between the different components of the injection module are shown in figure 3.1. Different characteristics of the injection module are summarized in table 3.1. Finally flow was passed through a nozzle (marked with "h" in the figure). The nozzle was used to increase the axial velocity of the flow, thus decreasing the remaining turbulence intensity at the jet exit. It also assured a flat hat velocity profile as shown below. The nozzle was drawn from a fifth order polynomial (equation presented in table 3.1) based on the suggestions of Morel (1975); Bell and Mehta (1988); Han *et al.* (2005); Tan-Atichat (1980) that is presented in figure 3.2. All instruments were placed on a static optic table to absorb vibrations and isolate the full device from environmental vibrations as well. A *DANTEC*

*Dynamics* traverse system controlled with a *Isel Schrittmotor* Controller C142-4 was used to move the hot wire probes with an accuracy of 1/160 mm. *DOSTMANN electronic* P795 high precision temperature probes were used to measure temperature with an accuracy of $\pm 0.001$ K.

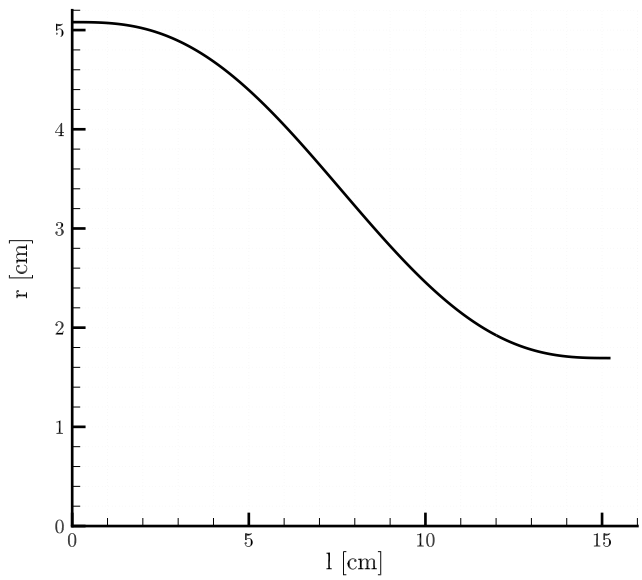


Figure 3.2: Axisymmetric nozzle section

## 3.5 Flow field characterisation

In the whole document, the axial coordinate $x$ is taken from the jet exit section, and we use the coordinate $r$ to quantify the radial distance form the jet axis, the origin coinciding with the center of the circular section.

Turbulent quantities are obtained through temporal statistics using the standard Reynolds decomposition which, for each spatial location, separates the mean $\overline{U}$ (which is a statistical moment of order one) from the fluctuating part $u'$ of the instantaneous velocity $u$:

$$u(t) = \overline{U} + u'(t) \tag{3.1}$$

where by definition $\overline{u'} = 0$. The two main quantities that will be analyzed in the following sections are $\overline{U}$ and the amplitude of the velocity fluctuations quantified by its root-mean-

Table 3.1: Summary of experimental setup

| Component | Dimensional Info |
|---|---|
| Perforated plate<br>Object "d" in the figure | 25 evenly distributed circular openings<br>Each openings diameter of 1.31 cm<br>PVC |
| Coarse screen<br>Object "e" in the figure | Wire diameter 1.6002 mm<br>Open area ratio 56%<br>Steel |
| Honeycomb<br>Object "f" in the figure | Length to diameter ratio 14.5<br>Aluminium |
| Fine Screen<br>Object "g" in the figure | Wire diameter 0.508 mm<br>Open area ratio 57%<br>Galvanized steel |
| Nozzle<br>Object "h" in the figure | Length to input diameter ratio 1.5<br>$r = 5.08 - 0.0095679l^3 + 0.00094172l^4 - 2.4717 \times 10^{-5}l^5$<br>Input diameter 10.16 cm<br>Area ratio 9<br>PVC |

square (which is a statistical moment of order two) defined as:

$$u_{\text{rms}} = \sqrt{\overline{u'^2(t)}}. \tag{3.2}$$

The turbulence intensity (also often referred to as the turbulence level) is defined as the ratio $u_{\text{rms}}/\overline{U}$ and is usually expressed in percentage. These turbulent quantities (mean and fluctuating velocity) will be studied for flow conditions that are completely determined by the Reynolds number of the jet, which is based on the jet exit characteristics:

$$Re = \frac{\rho U D}{\mu} \tag{3.3}$$

where $\rho$ is the density of the flow, $U$ the velocity at the jet exit section, $D$ the diameter of the jet and $\mu$ the dynamic viscosity of air.

### 3.5.1 Statistical convergence

A note concerning the computation of averages is first addressed here. A random turbulent signal is a superposition of the signature (the induced velocity field) of all the turbulent structures passing through the measurement point. When statistical moments have to be

obtained, a sufficient number of samples has to be recorded to reach statistical convergence so that averaged quantities do not depend on the number of samples (or acquisition time). The best way to determine this number remains to directly estimate it by simply analyzing the cumulative mean and root-mean-square of the turbulent quantities of interest as a function of the recording time. Figure 3.3 presents the convergence of $\overline{U}$ (figure 3.3a) and $u_{\text{rms}}$ (figure 3.3b) for velocity signals recorded at $x/D = 3$ for two radial locations, one in the center of the jet ($r/R = 0$) where the turbulence level is low, and another one in the mixing zone ($r/R = 1$) where the turbulence level is high.

As can be observed, statistics converge quite fast, and as expected $\overline{U}$ reach its terminal value more rapidly than $u_{\text{rms}}$, the data at $r/R = 1$ requiring more samples due to the higher fluctuation level. While it is better to use a longer time, in reality the temperature of the airflow can vary during the recording, especially if the acquisition time covers several minutes. Moreover, if a full velocity profile has to be measured by two different anemometers, they are performed sequentially so that the measurement time of each spatial point has to be minimized. Consequently, the acquisition time was chosen between 20 and 40 s, depending on the type of measurements (one point or a full profile), and was regularly verified.

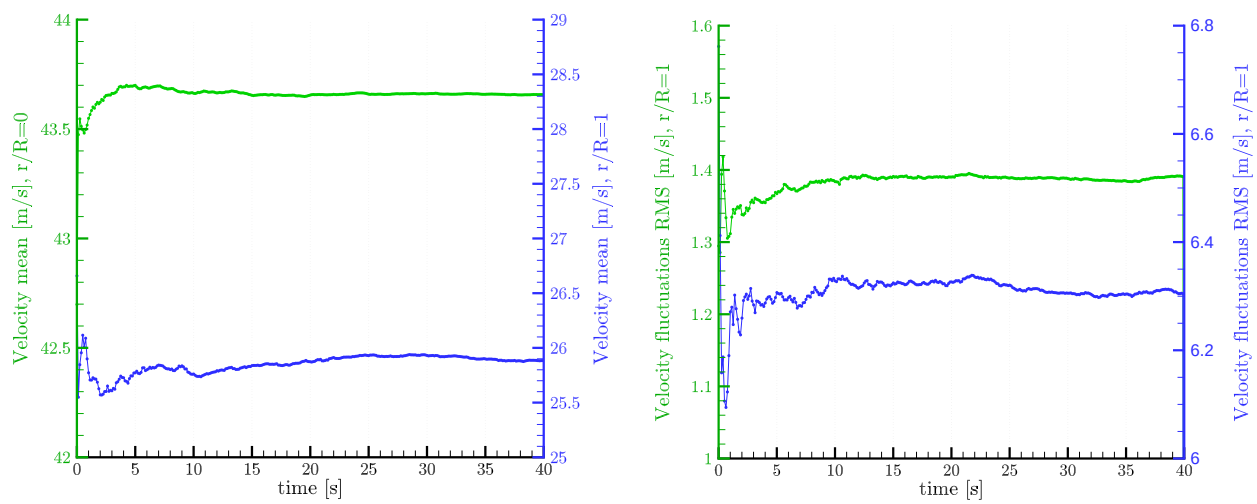


(a) Mean velocity $\overline{U}$

(b) Amplitude of velocity fluctuations $u_{\text{rms}}$

Figure 3.3: Convergence of mean and rms values at $r/R = 0$ (green line) and at $r/R = 1$ (blue line).

### 3.5.2 Exit velocity and turbulence profile

Before analyzing developed turbulence in section 5, we first present in figure 3.4a the velocity profile at the jet exit ($x/D < 0.1$) for $Re \simeq 80\ 000$, which is equivalent to a wire Reynolds number of $Re_w \simeq 11$. We can observe that the mean velocity is flat in the central region of the jet (maximum 1% variations in the range $r/R \leqslant 0.7$). The maximum deviation of the velocity from the axis value is 2.8 %, and comes from the design of the contraction. It can be reduced by changing the shape and smoothness of the contraction. However this deviation is acceptable for the purpose of this study.

The rms profile is presented in figure 3.4b. $u_{\mathrm{rms}}$ is relatively constant to a value of 0.9 % of the jet exit velocity in the central zone of the jet and abruptly increases as the measurement location reaches the lips of the jet ($r/R = 1$). This region is indeed the transition between the potential core where the velocity is constant and equal to $U$ and the ambient stagnant flow, and therefore is characterized by an intense shear. These results show that the flow is uniform in the central region of the exit section with a relatively small turbulence intensity. This calm flow region, called the potential core, will be the reference flow to calibrate all sensors used in this work, as will be shown in section 5.1. Now we will focus on the main objective of this study, the constant voltage anemometry.

The turbulence intensity of 0.9% in the central zone of the jet derives partially from the flow fluctuations and partially from the fan blade passage frequency. Power spectrum of the velocity signals recorded in that area shows a high energy peak in the same frequency as fan blade passage. For this reason, it can be said that the turbulence intensity represented here is higher than actual flow fluctuations due to the existence of fan blade resonance energy.

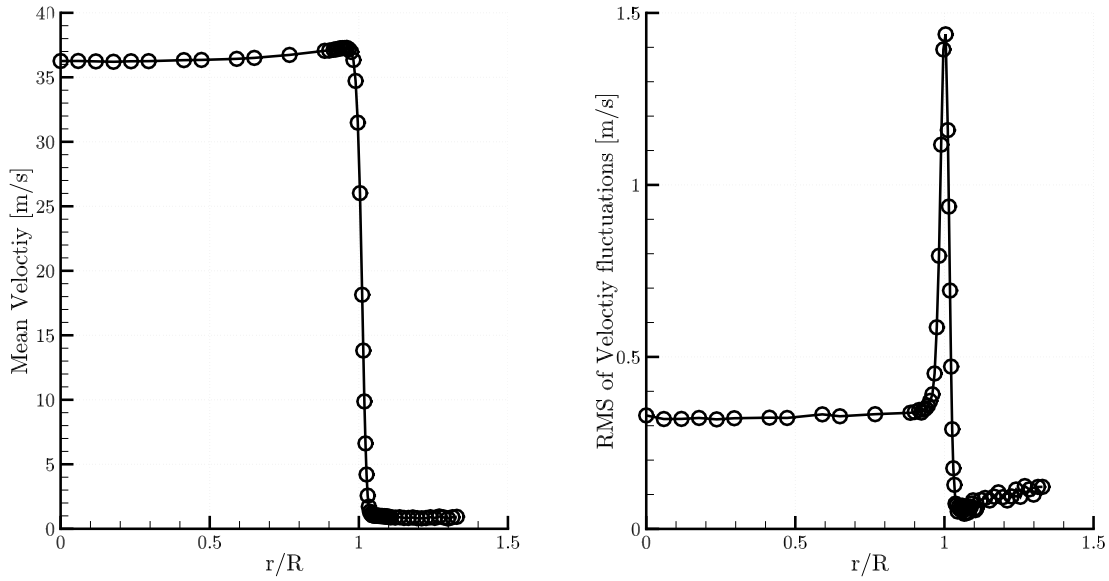


(a) Mean velocity $\overline{U}$

(b) Amplitude of velocity fluctuations $u_{\mathrm{rms}}$

Figure 3.4: Radial turbulent profiles at the jet exit section ($x/D < 0.1$).

# Chapter 4
# Constant voltage anemometer analysis

In this chapter we will study internal calibration and frequency response of the CVA system, as well as the thermal lag of the wire, and we will explain how to apply hardware and software compensations on the output voltages of the CVA anemometer.

## 4.1 Internal calibration of the CVA

In the CVA anemometry, the voltage across the wire, called $V_w$, is maintained constant to a value usually less than 1 V. This voltage heats the wire up to a temperature notably higher than the ambient one. The wire is cooled down by the flow and this changes the wire resistance, which leads to a change in the passing current. Note that with this working principle the overheat ratio of the wire is not constant and depends on the local flow velocity, which reflects the main difference with the CTA anemometer where the overheat ratio is held constant. The current passing through the sensing wire is also passed through a large resistance which produces a large voltage across it, making it easy to measure. This large voltage is called $V_s$ and is measured as the system output that will be used to obtain the instantaneous velocity through a calibration procedure. $V_s$ can be as high as 20 V depending on the flow velocity and wire voltage $V_w$. Since most of data acquisition devices accept voltages between $\pm 10$ V range, the $0 - 20$ V CVA output is not always easy to use. As a consequence, the CVA systems include another output where 10 V is subtracted to $V_s$, and this voltage is additionally passed through a low-pass filter whose the cut-off frequency can be adjusted to remove noise.

Writing Ohm and Kirchhoff's laws for the CVA circuit shown in figure 4.1, the relation between the wire resistance, the wire voltage $V_w$ and the response voltage of the system $V_s$ is described by equation 4.1 (which is driven in appendix A):

$$R_w + r_L = \frac{1}{aV_s/V_w + b} \tag{4.1}$$

in which coefficients $a$ and $b$ are measured by calibration for every circuit and are usually provided by the manufacturer.

Re-arranging equation 4.1 shows that there is a linear relation between $V_s/V_w$ and $1/R_w$. This relation is used in internal calibration of CVA systems. The internal calibration is done by placing different resistors in place of the wire, applying a $V_w$ voltage (usually around the value that we use for measurements), measuring $V_s$ and calculating $V_s/V_w$. Then, having a

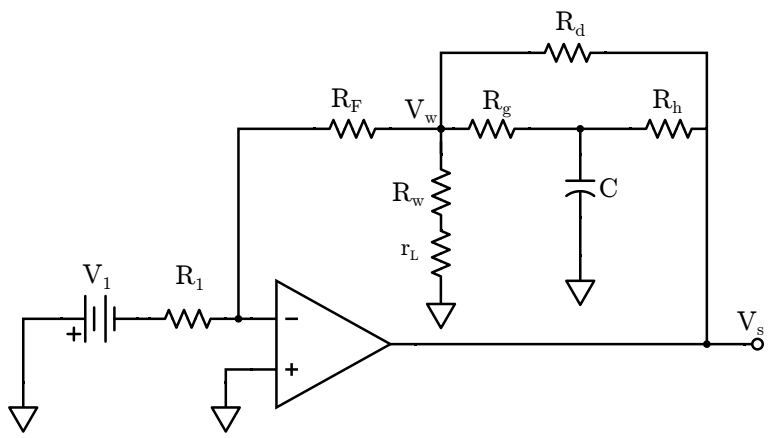


Figure 4.1: Electronic circuit of the CVA anemometer ($R_w$: sensing wire).

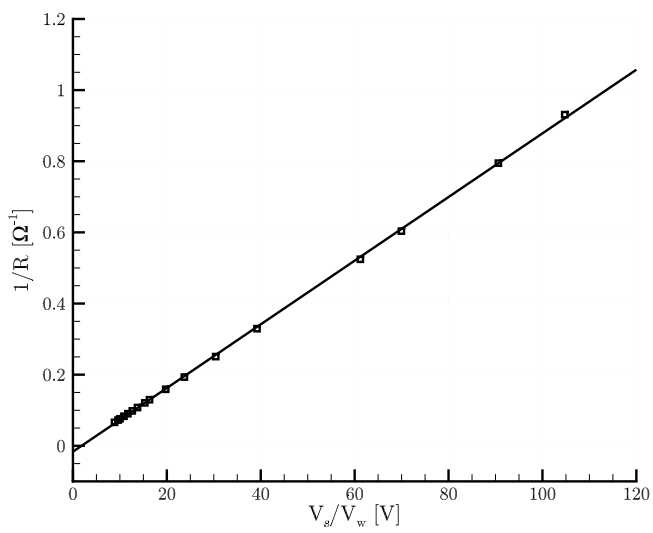


Figure 4.2: CVA Internal Calibration

sufficient number of points, the coefficients $a$ and $b$ can be estimated by a linear least square fit. Based on the calibration charts provided by the manufacturer, we have found out that they have not measured those coefficients with an adequate number of points. Also they have not calibrated all different outputs of the system. For example we have found that the constants in equation 4.1 are not the same for the non filtered $0 - 20$ V output and the filtered $\pm 10$ V output. Therefore we decided to re-calibrate all the available outputs of the CVA systems. An example of this internal calibration can be seen in figure 4.2. We used 15 resistors from 1 $\Omega$ to 15 $\Omega$ and applied a linear regression which gave us a coefficient

of determination $R^2$ in order of 0.999762 in the worst case. This internal calibration has been done for all outputs (including the TCM module[1]) used in measurements and no data from manufacturer calibration charts has been used. The exact values of coefficients $a$ and $b$ are listed in table 4.1. As can be seen, tests have been performed for three different anemometers and not only results from one instrument to the other, but also between the different channels of a single instrument, justifying the accurate measurements performed here. The difference of the coefficients between different channels and instruments is based on the fact that the electrical parts used in the circuits are not perfectly similar and their resistance and capacitance vary slightly. The difference between our measurements and values provided by manufacturer is from the fact that our calibration chart is plot using two times more calibration points.

Table 4.1: Values of coefficients $a$ and $b$ for CVA systems

| CVA number | Channel 1 Output $0-20$ V | | | Channel 1 Output $\pm 10$ V 512 kHz | TCM Module |
|---|---|---|---|---|---|
| | Manufacturer calibration charts | Measured | Difference | Measured | Measured |
| 1 | $a = 0.008503$<br>$b = -0.00978$ | $a = 0.008948$<br>$b = -0.016472$<br>$R^2 = 0.999762$ | 5.23%<br>68.42% | $a = 0.009009$<br>$b = -0.016075$<br>$R^2 = 0.999772$ | $a = 0.008801$<br>$b = -0.014920$<br>$R^2 = 0.999821$ |
| 2 | $a = 0.008467$<br>$b = -0.00936$ | $a = 0.008782$<br>$b = -0.014292$<br>$R^2 = 0.999897$ | 3.72%<br>52.69% | $a = 0.008887$<br>$b = -0.014535$<br>$R^2 = 0.999896$ | N/A |
| 3 | $a = 0.008479$<br>$b = -0.00950$ | $a = 0.008826$<br>$b = -0.015014$<br>$R^2 = 0.999853$ | 4.09%<br>58.04% | $a = 0.008932$<br>$b = -0.015231$<br>$R^2 = 0.999840$ | N/A |

## 4.2 Measurement of the wire cold resistance

Wire cold resistance is the resistance of the sensitive wire, when no electrical current is passing through it. Assuming that we know the physical characteristics of the metal with which the wire is made, its resistance should be a function of only the temperature through the wire temperature coefficient $\chi$:

$$R_2 = R_1[1 + \chi(T_2 - T_1)] \tag{4.2}$$

[1]This Module will be presented further in section 4.3

Where equation $R_1$ and $R_2$ are the wire resistances at wire temperatures $T_1$ and $T_2$ respectively. The temperature coefficient $\chi$ for the tungsten wire we used in our tests is 0.0036 $K^{-1}$. Knowing the resistance at temperature $T_1$, we can calculate the resistance of an arbitrary temperature $T_2$, which requires exact measurements of the initial resistance and both temperatures. Due to the fact that $\chi$ can change during the lifetime of the wire (for example, after using the wire with a high overheat ratio the metal might start oxidizing) the results might not be accurate. Then the wire cold resistance $R_a$ should be often measured with an additional temperature probe, which is not always possible to do. In iso-thermal measurements the cold resistance can change if the ambient temperature is changing, and it is known that in thermal anemometry this point is important (in water for example, a change of $\pm 10$ K in the fluid temperature leads to an error of 10% on the mean velocity). Obviously, in non iso-thermal flow, accurate CTA/CVA measurements would be far more difficult to obtain without appropriate temperature measurement systems. For these reasons some researchers tried to measure the wire cold resistance in-situ with the CVA anemometer by using the same probe used to capture velocity. The procedure is as follows.

Power dissipated by the sensing wire is defined by $P_w = R_w I_w^2 = V_w^2/R_w$. Sarma and Comte-Bellot (2002) proposed to define $P_w/(R_w - R_a)$ as a new output of the CVA system at each test point (instead of the usually used $V_s$ voltage) and conduct velocity calibration and measurements with this new parameter. We will call this parameter PDR (Power Dissipation Ratio) in this text, as they did in their article. Since an accurate measurement of the wire cold resistance is needed for each measurement point, they suggested to measure wire cold resistance locally by applying successively several very small $V_w$ voltages to the wire, then plotting $R_w$ as a function of $P_w$ and by extrapolating the data to where $P_w \to 0$ to estimate the value of the wire cold resistance. Their main arguments are that $V_w$ voltage across the wire can be rapidly changed without any problems since no additional circuit balancing is necessary, and that small values of $V_w$ (they suggested 10 mV) would not heat the wire significantly from the ambient temperature. With this technique, it appears possible to measure simultaneously the velocity and temperature on a flow specially non-homogeneous in temperature. This method has been implemented by (Truzzi *et al.*, 2002) in subsonic and by Comte-Bellot and Sarma (2001) in supersonic flow. However the minimum value of $P_w$ that Comte-Bellot and Sarma (2001) measured was higher than 2 mW. Our investigation showed that this method can not be implemented as easy as explained, due to technical limitations in CVA systems. We found out that as one decreases the value of $V_w$, decreasing $P_w$ to lower than $\sim$ 2 mW, the linear trend between $R_w$ and $P_w$ is not valid any more as shown in figure 4.3. Also, if we compare the results of the different CVA outputs, they diverge to different values.

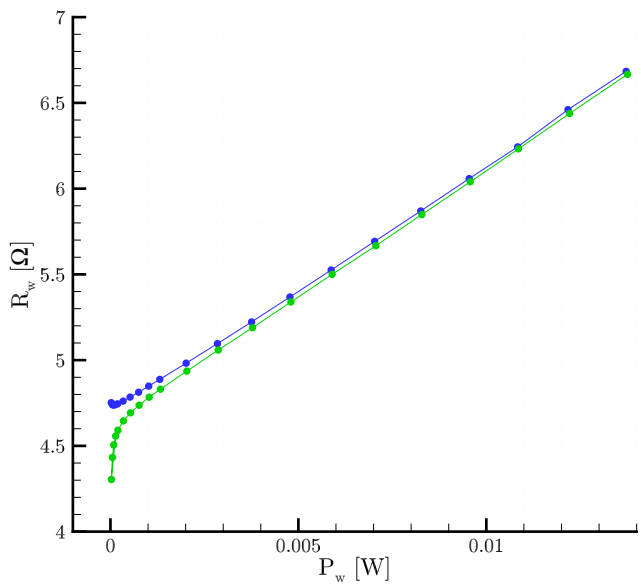


Figure 4.3: CVA, wire cold resistance estimation

In the example presented in figure 4.3, the 5 µm diameter tungsten wire was placed in the potential core of the jet, characterized by a uniform velocity and a low turbulence level. Based on the flow temperature and the measured wire resistance at ambient temperature, the wire resistance in the flow using equation 4.2 should be 4.751 Ω. Two different outputs from the same channel have been simultaneously recorded. One from the ±10 V output with a 512 kHz on-board low pass filter, the other from the non filtered $0 - 20\ V$ output.

While the value obtained from the different outputs should be the same since wire resistance is a physical characteristic of the wire that does not depend on the circuit used to measure it, results shown in figure 4.3 indicate that not only the filtered and non-filtered output results slightly differ, but also as $P_w$ is decreased, none of the outputs keep the linear relation between $R_w$ and $P_w$.

We were not able to explain this phenomenon that probably comes from the electrical circuit. However, since the procedure consists to find $R_a$ by estimating the ordinate value at the origin of the linear fit, it appears that even slight differences in the slope calculation can results in large discrepancies in the estimation of $R_a$. For example in the curve presented in figure 4.3, the estimation of $R_a$ can vary up to 1.57% based on the range of $P_w$ chosen to plot linear fit. This means that in the applications where an accurate value of $R_a$ is required, this method can not be relied on.

For this reason we decided to not use this method in our experiments and to calculate the wire resistance using equation 4.2. In this way there is no CVA circuit involved. A temperature probe was therefore used to measure the flow temperature (assuming the flow is iso-thermal) and the calculations were done using nominal values of the temperature coefficient $\chi$, which allows to correct the signals with changes in ambient temperature but not the wire oxidizing. However, the last phenomena occurs in a long period of time, which is not considered having a real effect on final results.

## 4.3 Investigation of the wire termal inertia

As seen in section 2.2, the output voltage $V_s$ of the CVA anemometer is related to the wire instantaneous resistance, that will be subsequently related to the instantaneous velocity through a calibration law. However, the sensitive wire is not perfect and has its own dynamic response to changes in velocity. Furthermore, the wire is not directly connected to the anemometer but instead the chain contains different elements that can contribute to affect the dynamic response of the whole system, and therefore the final estimation of the velocity. While it is not easy to estimate the influence of all these parameters, it is necessary to perform some corrections if the dynamic response of velocity is important, which is the case when the flow velocity has high frequency fluctuations, as in turbulent flows.

*The different components that can affect the dynamic response of the CVA anemometer can be divided in two main contributions: first the dynamic response of the tungsten wire, and second the dynamic response of the CVA electronic circuit. The first will be discussed in this section and the latter in section 4.4.*

The main phenomenon that affects the wire response is its thermal inertia. If we neglect the heat loss due to conduction to the sensor prongs, the dynamic response of the wire can be obtained from the energy balance between the heating of the wire coming from the current $I_w$ passing through it and its cooling due to the forced convection induced by the flow, which can be drawn from the first law of thermodynamics (this energy balance was detailed in equation 2.5 presented in section 2.2 to obtain the calibration law):

$$\frac{m_w c_w}{\chi R_a}\frac{dR_w}{dt} = R_w I_w^2 - (R_w - R_a) f(U), \tag{4.3}$$

where $c_w$ is the specific heat and $m_w$ the mass of the tungsten wire, and $f(U)$ a function that characterizes the physical law that relates the change of resistance with the flow velocity $U$ (the component normal to the wire). An ideal wire is a wire that is always in equilibrium with the flow and so has zero thermal inertia (no thermal lag), therefore the energy balance

becomes:

$$0 = R_w^* I_w^{*\,2} - (R_w^* - R_a) f(U), \tag{4.4}$$

where the asterisks are used to characterize the ideal wire (Comte-Bellot *et al.*, 2004). Since the voltage $V_w$ is constant, we have:

$$(R_w + r_L) I_w = (R_w^* + r_L) I_w^*, \tag{4.5}$$

where $(R_w + r_L)$ is the full resistance over which $V_w$ is imposed, and contains the resistance $R_w$ of the wire alone but also the lead resistance $r_L$ which is the total resistance of the different elements connecting the wire to the anemometer. By eliminating $f(U)$ between equations (4.3) and (4.4), we obtain:

$$\frac{1}{V_w^2} \frac{m_w c_w}{\chi R_a} \frac{dR_w}{dt} = \frac{R_w}{(R_w + r_L)^2} - \frac{R_w^*}{(R_w^* + r_L)^2} \frac{R_w - R_a}{R_w^* - R_a} \tag{4.6}$$

Comte-Bellot *et al.* (2004) further developed this equation by writing every quantity as the sum of a mean value (noted with an overbar) and a fluctuating part (noted with a prime). In particular, we have $R_w = \overline{R_w} + r_w'$ and $R_w^* = \overline{R_w^*} + r_w'^*$, and assuming small velocity fluctuations (*i.e.* $r_w' \ll R_w$ and $r_w'^* \ll R_w^*$), the first order differential equation (4.6) can be linearized to give:

$$M_{\mathrm{CVA}} \frac{dr_w'}{dt} + r_w' = r_w'^* \tag{4.7}$$

which is analogous to the transfer function of a first-order system. The coefficient $M_{\mathrm{CVA}}$ therefore appears as a time constant that includes the effect of the wire and of the connecting leads, and can be expressed as:

$$M_{\mathrm{CVA}} = \frac{m_w c_w}{\chi R_a} \frac{1}{V_w^2} (\overline{R_w} + r_L)^2 \frac{\overline{\alpha_w}}{1 + 2\overline{\alpha_w}} LM, \tag{4.8}$$

where $\overline{\alpha_w}$ is the mean overheat ratio of the wire and $LM$ is the lead factor defined by Comte-Bellot *et al.* (2004) as:

$$LM = \left[ 1 + \frac{r_L}{R_a(1 + \overline{\alpha_w})} \right] \left[ 1 + \frac{r_L}{R_a(1 + \overline{\alpha_w})(1 + 2\overline{\alpha_w})} \right]^{-1}. \tag{4.9}$$

In reality, equation (4.7) cannot be strictly considered as a first-order transfer function because the time constant $M_{\mathrm{CVA}}$, which is a critical term in relating a real wire resistance to the ideal wire resistance, depends on several parameters. In particular, $M_{\mathrm{CVA}}$ depends on the wire physical properties (represented by the term $m_w c_w / \chi R_a$) but also on some flow

characteristics, including the temperature but also the local flow velocity through the overheat ratio.

In practice, however, we can generally assume that the value of $M_{\mathrm{CVA}}$ depends mainly on the local mean flow conditions, so that the time response of the wire can indeed be modeled as a first-order system providing that a mean velocity can be defined (the average is constant over time) and known at each measurement point, an hypothesis that for example fails in oscillating flows. To determine $M_{\mathrm{CVA}}$, it is possible to impose a step either in velocity or in current which is equivalent to a step in heat convection assuming the amplitudes remain small. For example, by focusing a laser beam the the flow upstream of the wire can be pulsatively heated. One can also physically oscillate the wire between a hot and a cold zone as explained by (Berson *et al.*, 2010a).

All these methods are based on the fact that the time constant of the wire can be measured from its resistance change when the step velocity change occurs. The step velocity change can also be simulated by a step change in the wire temperature or current, which is easily achieved by injecting a step voltage through a resistance connected to the wire thanks to an additional circuit. The advantage of this technique is that the time-constant can be measured *in situ*. For this, the CVA system is equipped with an on-board circuit, called the time constant measurement (TCM) module, which is suited to feed the wire with a square wave voltage signal (in addition to a pre-defined constant voltage $V_w$) leading to a step change in the wire temperature. This results in a change of the wire resistance (seen as a change in the output voltage $V_s$) in the form of a first order response. The TCM module is furthermore specially designed to separate the wire response from the circuit response (Sarma, 1998), so that the contribution of these two sources can be accurately determined through equations (4.8) and (4.9).

The TCM module feeds the wire with a square wave voltage with the frequency of $16.74 \pm 0.01$ Hz. Generally, the time constant is determined by connecting the module to an oscilloscope. A typical square wave response is shown in figure 4.4. As the wire is assumed to behave as a first-order system, its response has the form of an exponential function and $M_{\mathrm{CVA}}$ is determined as the time the voltage takes to decrease $1 - e^{-1} \simeq 63\%$ from its maximum value. In practice, however, we have to perform this test in the same conditions as the mean flow, but with the presence of high flow fluctuations and noise, the determination of $M_{\mathrm{CVA}}$ cannot be done. For this reason, to better characterize the time constant, the wire is placed in the potential core of the jet at a velocity close to that of the measurement where the flow fluctuations and noise is lower. This allows to considerably reduce the flow fluctuations. Furthermore, we decided to record $M_{\mathrm{CVA}}$ for several steps and then perform phase-averages of a large number of signals to obtain a time constant estimation. Since this cannot be easily

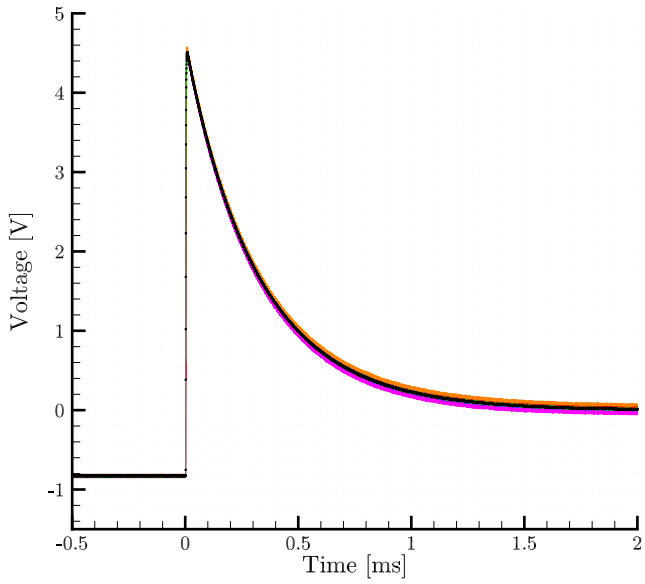


Figure 4.4: Sample of several responses (colored lines) to the square wave test as well as the phase-averaged response (black line). Note that one point over 4 is presented in the phase averaged response

done on an oscilloscope, this was achieved on an acquisition card able to acquire voltage samples at a sufficiently high acquisition frequency (15 MHz) to capture the velocity peak, shown in figure 4.4, with a sufficient resolution (16 bit, 0.1526 mV). After several tests, we finally obtain satisfaction with a digitizer card from National Instruments.

A sample of several step responses as well as the phase-averaged response can be seen in figure 4.4. Phase averaging was done by averaging the response voltage at every step time (time passed from the start of a step) over different steps. While efficient, this method was however very time consuming since it has to be repeated for several mean velocities. Our calculations indicated that the value of $M_{\mathrm{CVA}}$ calculated from the phase-averaging of $\sim 200$ step signals is very close to the value of the arithmetic mean of the $M_{\mathrm{CVA}}$ values individually determined for each step. For this reason, we decided to use this alternative to speed-up the determination of the time constant (the reason is mainly because the flow temperature is not constant during long measurements). The convergence of $M_{\mathrm{CVA}}$ with the number of samples used to calculate the mean value $\overline{M_{\mathrm{CVA}}}$ can be analyzed from figure 4.6. Values have been acquired in the potential core of the jet at a constant temperature (verified by temperature probes). In the example shown, a minimum number of 1700 steps was necessary to reach a statistically converged time constant, which requires $\sim 100$ s of acquisition time for each

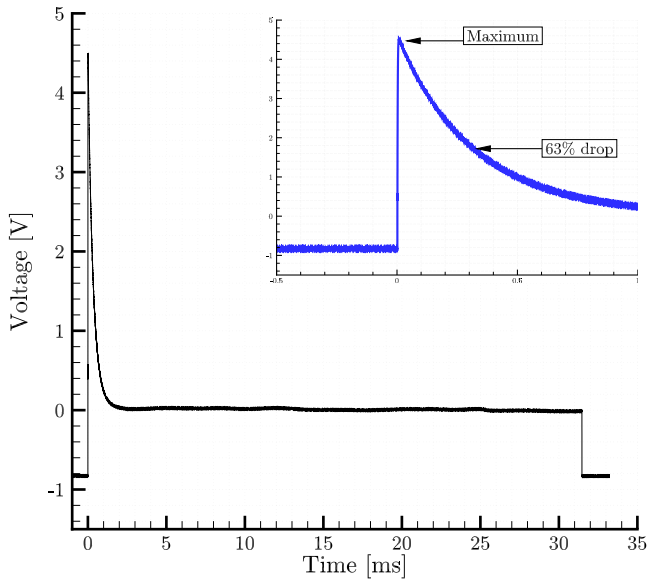


Figure 4.5: Sample of a wire response to square wave test. Inset: Closer look at the same graph, $M_{\mathrm{CVA}}$ is the time from maximum untill 63 % drop in the voltage (in this example it is $\simeq 3.2 \times 10^{-4}$ s)

mean velocity.

Equation 4.8 indicates that $M_{\mathrm{CVA}}$ can also be written under this form:

$$M_{\mathrm{CVA}} = \frac{m_w c_w}{\chi}\ h(V_w, R_a, \overline{R_w}, r_L, \overline{\alpha_w}), \tag{4.10}$$

*i.e.* as the product of $m_w c_w/\chi$, which only depends on the wire characteristics, with a function $h$ that only depends on electronic and flow parameters. For the Dantec 55P11 probes used in this study (5 $\mu$m by 1.25 mm cylindrical wire), assuming that for tungsten $m_w = 4.7369 \times 10^{-10}$ Kg, $c_w \simeq 140$ J Kg$^{-1}$K$^{-1}$ and $\chi = 0.0036$ K$^{-1}$, we obtain $m_w c_w/\chi \simeq 1.8421 \times 10^{-5}$ J, a value that should be constant for all wires of the same type. Figure 4.7 shows $M_{\mathrm{CVA}}$ measured in the potential core of the subsonic jet flow as a function of $h$ (*i.e.* for different velocities) for one probes. As expected, $M_{\mathrm{CVA}}$ is a linear function of $h$, but the slope of the curves differ by 40% from the theoretical value. This difference can however be explained by the fact that the nominal value has been calculated based on the wire being perfectly cylindrical with known dimensions and density, and other physical characteristics being known and accurate. In reality the wires are manufactured by hand so that their characteristics can differ from case to case.

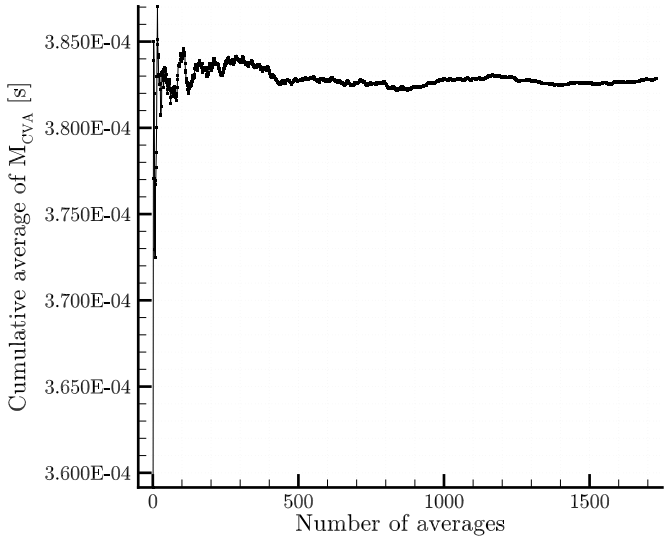


Figure 4.6: Convergence of the $M_{\mathrm{CVA}}$time constant with the number of averages.

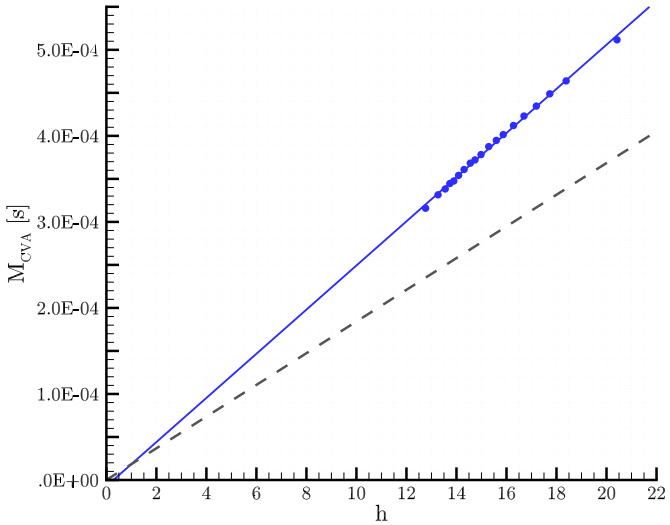


Figure 4.7: Evolution of $M_{\mathrm{CVA}}$ as in equation (4.10). Dashed line shows the nominal value

Now that we have a liable and repeatable method to measure $M_{\mathrm{CVA}}$, we are able to measure the thermal lag of the wire sensors at the desired flow conditions. Knowing $M_{\mathrm{CVA}}$,

it appears also possible to compensate the thermal inertia of the wire resistance and to correct voltage signals to obtain the true velocity signal. However, we have investigated here only the frequency response of the wire. The frequency response of the anemometer has also to be taken into account before applying a full compensation, which is the subject of the next section.

## 4.4 Compensation for the wire thermal inertia

The frequency $f_w = 1/(2\pi M_{\mathrm{CVA}})$ is the limit beyond which the sensing wire cannot correctly responds to resistance fluctuations, which means a maximum bandwidth of the order of 500 Hz to 700 Hz (Sarma, 1998). For velocity or temperature fluctuations at higher frequencies, the wire response, due to the thermal inertia, is altered. To increase this physical limit, it is possible to compensate by amplifying the fluctuations, which can be realized by adding an appropriate electronic circuit.

The CVA anemometer uses a resistor–capacitor (RC) combination as an operational amplifier feedback circuit to increase the hot–wire frequency bandwidth. Details about this circuit, shown in figure 4.8, is presented in Sarma (1998). The RC circuit simply acts as a first order amplifier that increases the system response to frequencies higher than $f_{\mathrm{TC}}$ at a rate of 20 dB/decade, which results to extend the bandwidth up to hundreds of kHz, and this is sufficient to resolve most of fluid flows, including supersonic turbulence. The parameter $\mathrm{TC} = 1/(2\pi f_{\mathrm{TC}})$ is called the circuit time constant (TC) and is solely defined by the physical characteristics of the circuit through the following relation (Sarma, 1998)

$$\mathrm{TC} = \frac{C R_g R_h}{R_g + R_h} \tag{4.11}$$

This RC–circuit will be also be called the *hardware compensation* in the rest of the text.

The transfer function of the CVA circuit is modified by the RC–circuit. Before presenting it, it is first convenient to work with voltages instead of resistance fluctuations since this is what we acquire. The relation between $V_s$ and $R_w$ follows from figure 4.8a as shown by (Sarma, 1998):

$$V_s = V_w \left[ 1 + \frac{R_g + R_h}{R_F} + \frac{R_g + R_h}{R_w + r_L} \right]. \tag{4.12}$$

If again we assume that all fluctuations in resistance and voltage are small compared to their mean values ($r'_w \ll \overline{R_w}$, $v'_s \ll \overline{V_s}$), this equation is linearized by Berson *et al.* (2009) to give:

$$v'_s = -V_w \frac{R_g + R_h}{(\overline{R_w} + r_L)^2} r'_w \tag{4.13}$$

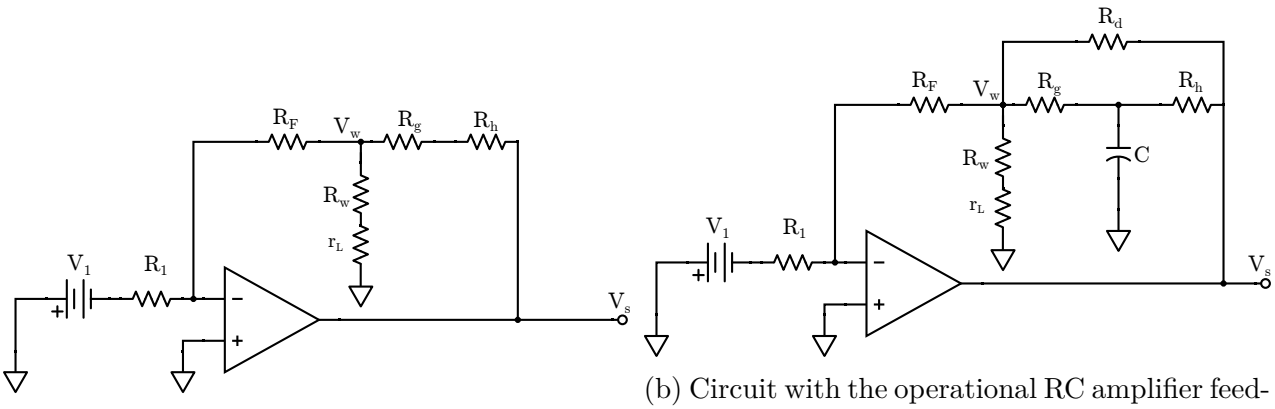


(a) Basic Circuit

(b) Circuit with the operational RC amplifier feedback circuit

Figure 4.8: CVA anemometer circuits.

which shows that voltage fluctuations are proportional to resistance fluctuations so that from equation 4.7, which reflects the thermal inertia of the wire, we can write the following first–order differential equation for $v_s'$:

$$v_s'^{*} = v_s' + M_{\mathrm{CVA}} \frac{dv_s'}{dt} \tag{4.14}$$

where $v_s'^{*}$ would be the voltage obtained with an ideal probe. Now if we introduce the RC-circuit shown in figure 4.8b, the modified voltage, called $v_{s_{\mathrm{TC}}}'$, can also be obtained from a first–order differential equation with the time constant TC:

$$v_{s_{\mathrm{TC}}}' = v_s' + \mathrm{TC} \frac{dv_s'}{dt}. \tag{4.15}$$

By combining equations 4.14 and 4.15, we finally obtain:

$$v_s'^{*} + \mathrm{TC} \frac{dv_s'^{*}}{dt} = v_{s_{\mathrm{TC}}}' + M_{\mathrm{CVA}} \frac{dv_{s_{\mathrm{TC}}}'}{dt} \tag{4.16}$$

which provides the exact correction to apply to $v_{s_{\mathrm{TC}}}'$ in order to recover the true signal. We can also re-arrange this equation to the following form:

$$v_{s_{\mathrm{TC}}}' = v_s'^{*} + \left[\mathrm{TC} - M^{\mathrm{CVA}}\right] \frac{dv_s'}{dt} \tag{4.17}$$

which includes both the effects of the wire thermal lag and the RC operational amplifier circuit on the output voltage. It is clear that if TC is chosen to exactly compensate the wire time lag, *i.e.* $\mathrm{TC} = M_{\mathrm{CVA}}$, then the output voltage fluctuations equal the ideal voltage,

which would results in a perfect hardware compensation. However, in practice, this cannot be achieved since $M_{\mathrm{CVA}}$ depends on the flow conditions. When the wire time constant is not equal to the designed TC value, the RC–circuit will either over-compensate or under-compensate the signals. In those situations the true signal can still be recovered using an additional compensation, called the *software compensation* since this is performed as a post-processing treatment. The following diagram finally summarize the full compensation procedure:

$$U \xmapsto[\text{thermodynamics}]{\text{First law of}} R_w^* \xmapsto[\text{thermal inertia}]{\text{Wire}} R_w \xmapsto[\text{including TC}]{\text{Circuit transfer function}} v'_{s_{\mathrm{TC}}} \xmapsto[\text{software compensation}]{\text{Hardware or}} v'^*_s$$

$$U \xleftarrow{\text{Calibration equations}} R_w^* \xleftarrow{R=1/(a\frac{V_s}{V_w}+b)} v'^*_s$$

The correction for TC is more easily performed in the frequency domain, since by taking the Fourier transform of equation 4.17, we obtain the Fourier transform of the corrected signal $v'_{s_{\mathrm{corr}}}$:

$$v'_{s_{\mathrm{corr}}}(\omega) = v'_{s_{\mathrm{TC}}}(\omega)\left[\frac{1 + j\omega M_{\mathrm{CVA}}}{1 + j\omega \mathrm{TC}}\right] \tag{4.18}$$

where $\omega$ is the angular frequency and $j = \sqrt{-1}$. The same compensation can however be done in the time domain as well. For a discrete voltage signal acquired at a sampling rate $f_s$, Comte-Bellot and Sarma (2001) proposed to use a backward finite difference to approximate the time derivative at time step $i$:

$$v'_{s_{\mathrm{corr}}}(i) = \frac{v'_{s_{\mathrm{TC}}}(i) + f_s[M_{\mathrm{CVA}}(v'_{s_{\mathrm{TC}}}(i) - v'_{s_{\mathrm{TC}}}(i-1)) + \mathrm{TC}v'_{s_{\mathrm{corr}}}(i-1)]}{1 + \mathrm{TC}f_s}. \tag{4.19}$$

The corrections in time and frequency domain are identical, and we chose time domain correction. Finally, as the time constants do not change the mean voltage, the total voltage $V_{s_{\mathrm{corr}}}$ is:

$$V_{s_{\mathrm{corr}}} = V_s + v'_{s_{\mathrm{corr}}}$$

and corresponds to the signal used to derive the instantaneous ideal wire voltage.

For this post processing the exact value of TC, which should be provided by the manufacturer, is required. However, by using the prescribed values, results were not satisfactory enough. The CVA systems have in fact two different TC settings so two values can be chosen. These two TC settings (called TC1 and TC2) are parallel and at each time only one of them is in use. The reason to place two parallel circuits is to give more flexibility to user. In order to obtain accurate results, a special set-up has been developed to measure both time constants. The best way to measure the value of TC would be using the Bode magnitude plot. This plot represents the gain in amplitude (magnitude) at each frequency. Various test signals can be

used to determine the bode plot of a system, including one impulse signal, a frequency sweep signal or a series of sinusoidal signals at different frequencies. Even if this latter procedure needs more time because one signal contains only one frequency (contrary to non-sinusoidal signals that cover a characteristic range of frequencies), these tests were undertaken as they give the most accurate results. They consists in feeding the system with successive sinusoidal signals with increasing frequencies while keeping the amplitude unchanged, then analyzing the gain with the frequency.

To conduct the sine wave tests, the circuit presented by Sarma *et al.* (1998) shown in figure 4.9 has been used. A typical axial-lead 5 Ω resistor was used instead of the hot-wire to keep the resistance constant during the tests and to eliminate thermal inertia. The wire voltage $V_w$ was fixed at 0.45 V for all measurements. The sine wave signal was injected using a DAQ system (National Instruments NI PXI-6229, connected using SCB-68 screw terminal connector block). Both filtered (±10 V, 512 kHz filter) and non-filtered ($0 - 20$ V) outputs of the CVA system have been recorded. The frequency of sine waves was spanned between 1 Hz to 5 kHz. At every measurement point, after acquiring a sufficient number of cycles, the amplitude of the power spectrum at the excited frequency was obtained.

The sine wave tests have been conducted several times for two different anemometers, and for both TC1 and TC2 on-board settings, and the whole results are shown in figures 4.10-4.12. On the Bode plots, the gain is equal to 1 at low frequencies and the RC amplifier circuit is not acting. As the frequency increases, the gain start to increase, then reach a linear trend (in a log–log plot) until a limit that corresponds to the maximum bandwidth of the system. This maximum bandwidth was not the subject of this study but Sarma *et al.* (1998) showed that it corresponds to a constant. By definition, the cut-of frequency $f_{\mathrm{TC}}$ is defined at +3 dB. A linear rate of 20dB/dec is observed, as expected for a first order system. We also observe a great repeatability of the results. The main error in estimating TC comes from the frequency span between two consecutive frequency values before and after intersecting the horizontal 3 dB line. Based on the results presented, it was estimated that the repeatability in the measurements of TC is better than 1%. These results as well as the values indicated by the manufacturer for both systems have been summarized in table 4.2, which indicates that the difference between the manufacturer estimations and our measurement are close (2%) for TC1 but can reach $\sim 27\%$ for TC2.

## 4.5 Results

Now the time constants of the sensitive wire $M_{\mathrm{CVA}}$ and of the CVA system TC1 and TC2 have been determined, in this section we will perform preliminary corrections to evaluate the

Table 4.2: TC values obtained from the measurements compared with the manufacturer data.

| | | TC1 setting | TC2 setting |
|---|---|---|---|
| CVA 1 | Frequency from Sine wave test | $519 \pm 4$ Hz | $2175 \pm 15$ Hz |
| | Equivalent TC Value | $0.3064 \pm 0.87\%$ ms | $0.0732 \pm 0.69\%$ ms |
| | Manufacturer TC value | 0.3 ms | 0.1 ms |
| CVA 2 | Frequency from Sine wave test | $518 \pm 3$ Hz | $2162 \pm 7$ Hz |
| | Equivalent TC Value | $0.3073 \pm 0.58\%$ ms | $0.0736 \pm 0.34\%$ ms |
| | Manufacturer TC value | 0.3 ms | 0.1 ms |

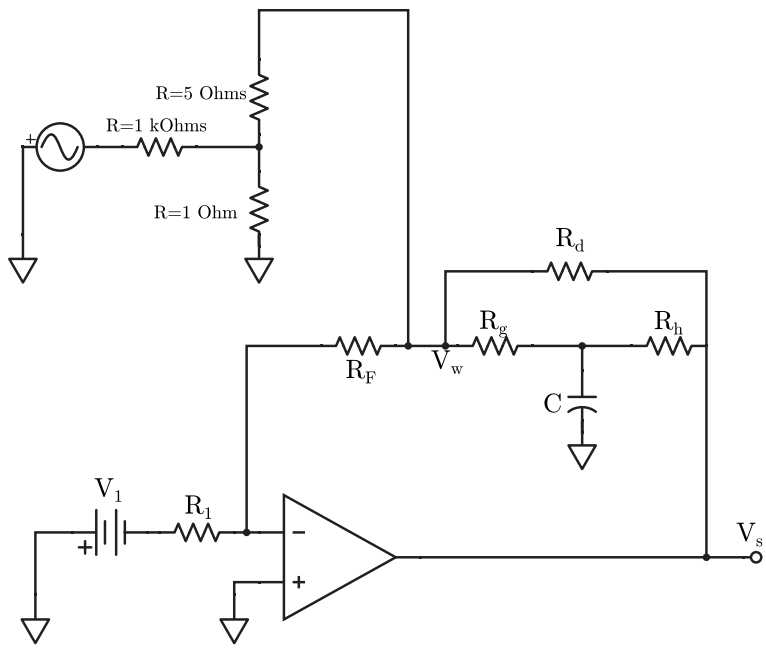


Figure 4.9: Sine wave test setup

validity of the results obtained in this chapter.

The TCM module of the CVA system is specially designed to estimate $M_{\text{CVA}}$ by providing a square voltage signal and by separating the wire response from the circuit response. If we want to measure the wire response alone, no external amplification has to be done. This is why this module is not equipped with the operational RC amplifier shown in figure 4.8a. So if the square wave injection is turned off, the TCM module works as a normal CVA system but without hardware compensation. The TCM module output is therefore only affected by the wire response, *i.e.* is only sensitive to the wire thermal inertia. The other channels of the CVA system have the complete circuit shown in figure 4.8b, which means that they incorporate a partial compensation with either the time constant TC1 or TC2. Since all

the channels of the system are assumed to have twin circuits, in the following text the TC0, TC1 and TC2 output channels will refer to the output without hardware compensation, with partial hardware compensation with TC1 and with partial hardware compensation with TC2, respectively.

At this stage a preliminary test can be performed to check the validity of the values of TC1 and TC2 that have been obtained, by simply correcting the TC0 signal by a software compensation and comparing to two other outputs. TC0, TC1 and TC2 voltages $V_s$ have been recorded in the mixing zone of the turbulent jet. To eliminate any wire effect in the anemometer responses, the same wire (a Dantec 55P11 5 µm tungsten wire), support and connecting cable have been used and therefore all signals cannot be acquired simultaneously but have been acquired successively by keeping the same flow conditions. The flow temperature has also been monitored and was found to be constant with less than 0.1°C variation during the tests. Since a constant wire voltage of 0.45 V has been used for all tests, this means that the wire mean resistance was also similar.

Each temporal voltage signal has been recorded with an acquisition frequency of 100 kHz during 60 s, and results are shown in figure 4.14 which presents the power spectral densities of the fluctuating voltage signals. The TC0 spectrum shows a typical spectrum with the energy concentrated at low frequencies. The maximum is observed at $f \sim 100$ Hz and the amplitude then decreases as the frequency increases beyond this value, which reflects the turbulent content of velocity fluctuations in the mixing zone. The noise level can be detected as a plateau in the TC0 spectrum shape at high frequencies, and that is reached at $\sim 8$ kHz. This plateau does not mean that no velocity fluctuations occur beyond this frequency, but that we have reach the electronic noise level of the anemometer.

To better understand the consequence of using the hardware compensation, figure 4.14 also presents two additional curves built with the TC1 and TC2 signals corrected with the TC1 and TC2 values obtained in section 4.4 in order to recover the signals that we would have been obtained without any hardware compensation, *i.e.* by using equation 4.19 with $M_{\mathrm{CVA}} = 0$. As we can observe, the resulting spectra matches the original TC0 signal. This validates that the measured values for the operational amplifier time constants presented in table 4.2 are sufficiently accurate. We can also clearly observe that the apparent noise level is lower for the TC2 signal, and even slightly lower when the TC1 time constant is chosen, however the spectral content is not sufficiently rich to more clearly differentiate the effects between TC1 and TC2 (this would have been the case for a higher Reynolds number that we cannot reach here). We can therefore conclude that the partial hardware compensation allows to shift the maximum sensitive frequency response of the system to higher frequency values, as observed in the example shown in figure 4.14. In the case when velocity fluctuations

reach higher frequencies that in our example, like in supersonic flows, the CVA anemometer offers a characteristic frequency response that other available anemometers cannot reach.

In figure 4.14 a peak is observed in a bandwidth centred around $\simeq$60 Hz. This peak is not related to the measurement instrument and is due to the largest turbulent structure passage frequency, called coherent structure. The energy of this structure passes to smaller scale structures as we move further from jet exit, so this peak is not observed in final measurements. A comb of harmonics of 8kHz are seen in both TC1 and TC2 results in the high frequency zone. These harmonics are more dominant in TC2 graph. We have no explanation on the origin of these harmonics, but as they are in a very low energy level (order of -12 decades) they have no effect on the mean and RMS values measured by the CVA. Note that the axis in figure 4.14 are in logarithmic scale.

Now that TC values have been confirmed, the next step would be to evaluate the $M_{\mathrm{CVA}}$ time constant to recover the full fluctuating velocity signal from the voltage signal by performing $M_{\mathrm{CVA}}$ and TC corrections. However, at this stage, we will need to compare our results to a reference velocity signal. For this, we have preferentially to use another technique to measure the fluctuating velocity, and the choice was to use a constant temperature anemometer because it is more widely. However, the CTA anemometers, despite working on a different working principle, have also their own frequency response and limits. This is investigated in appendix B.

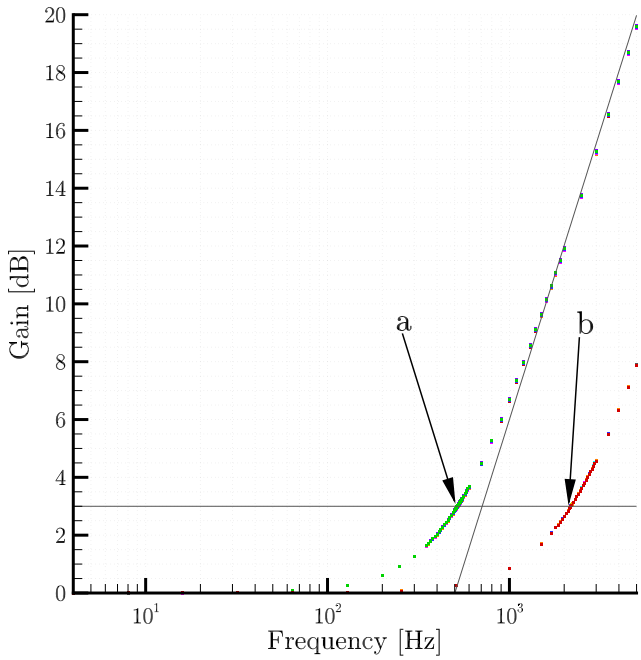


Figure 4.10: Bode plot for the CVA 1, for both TC1 (point "a") and TC2 (point "b") settings, with the constant 3 dB line plotted in grey for reference. The inclined line has 20dB/dec slope.

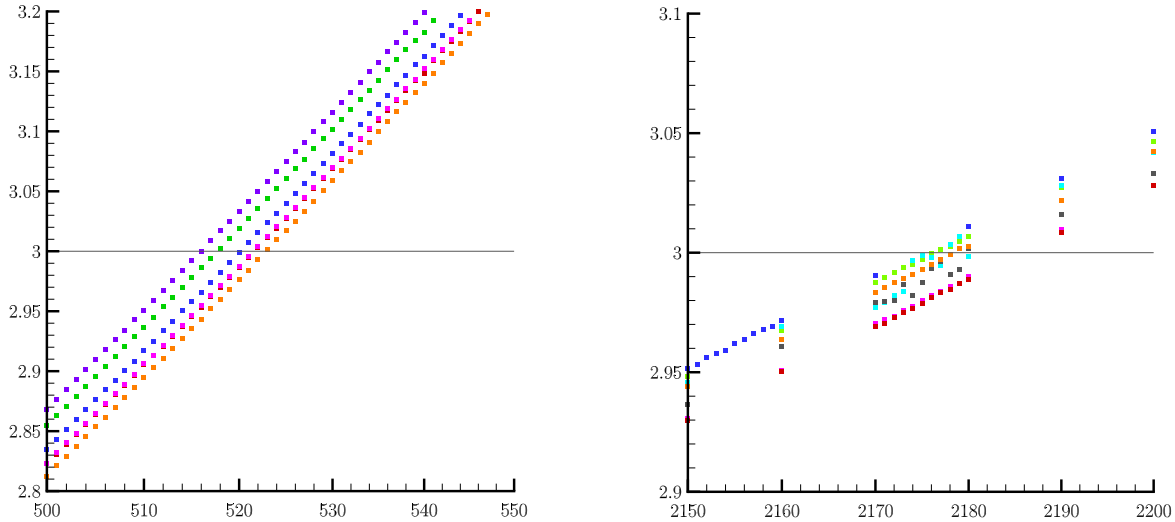

(a) Detailed view of the point "a" (TC1)

(b) Detailed view of the point "b" (TC2)

Figure 4.11: Detailed views of figure 4.10.

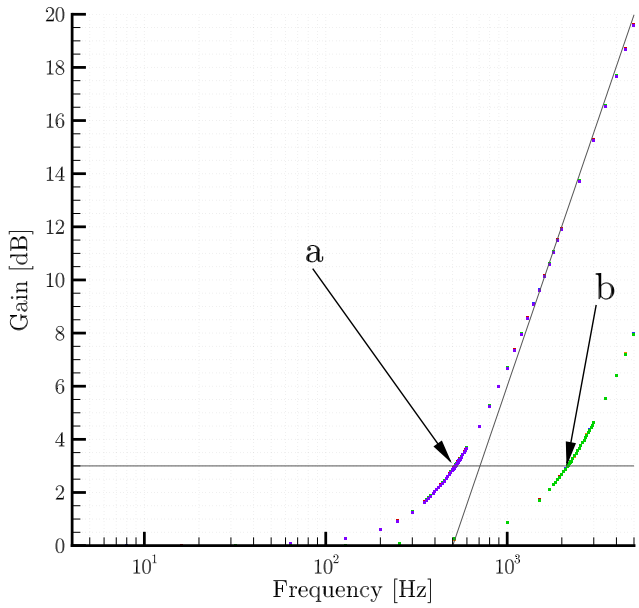


Figure 4.12: Bode plot for the CVA 2, for both TC1 (point "a") and TC2 (point "b") settings, with the constant 3 dB line plotted in grey for reference. The inclined line has 20dB/dec slope.

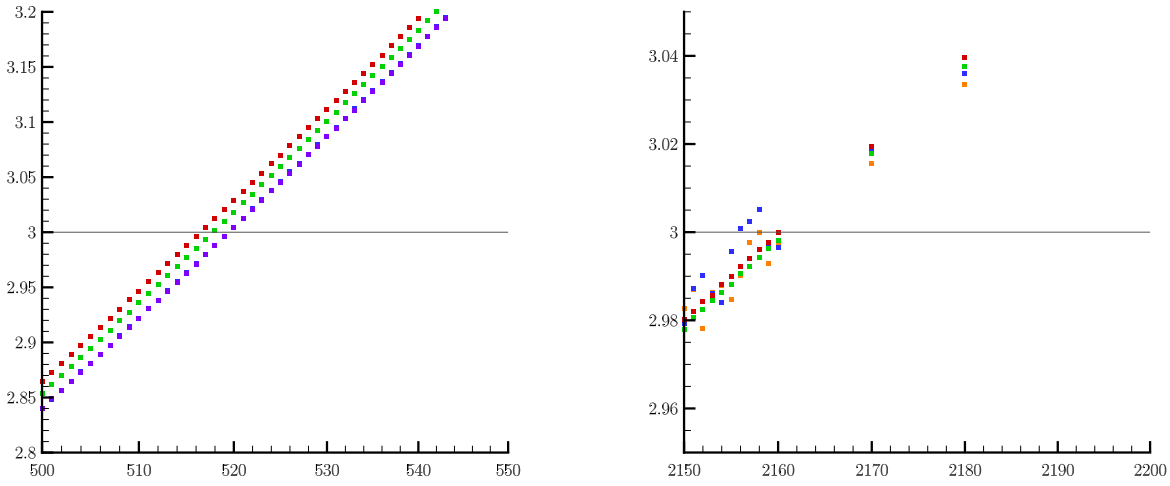

(a) Detailed view of the point "a" (TC1)

(b) Detailed view of the point "b" (TC2)

Figure 4.13: Detailed views of figure 4.12.

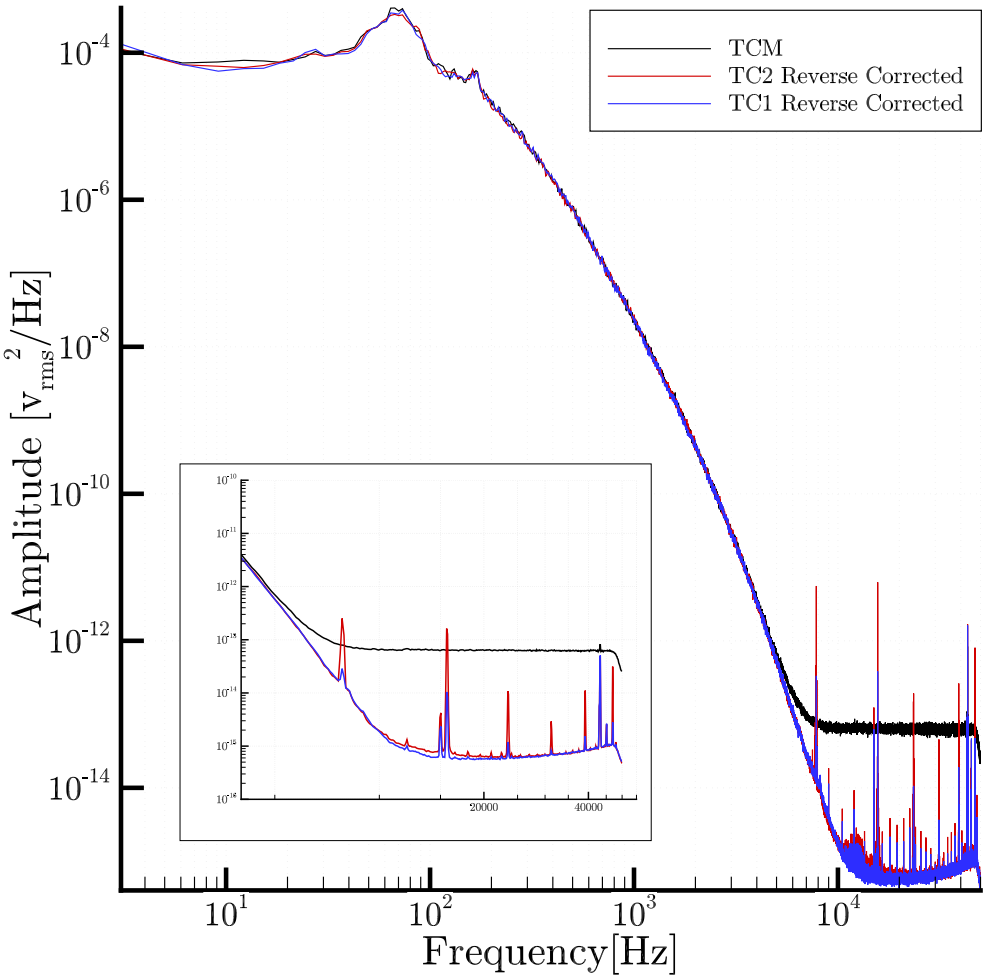


Figure 4.14: Power spectral density of voltages from Ch1 and TCM outputs of same instrument. Inset: Closer look at the high frequency zone

# Chapter 5
# Turbulent flow measurements

In the previous section we have detailed all the corrections required to recover the true signals from the measured ones. In this section we will present the results in order to validate the full procedure. In particular we will investigate the effect of the signal compensation on the turbulent averaged quantities as well as on the power spectra of velocity fluctuations. First, the calibration method to relate the anemometer output voltage to velocity is explained. This method will permit to compare data from different instruments by converting them to velocity data, which has a more physical meaning.

## 5.1 Calibration procedure

There is no universal law to relate the anemometer output voltage to the flow velocity since each wire has its own response depending on its shape, size, etc. As a consequence, each wire connected to a specific anemometer channel needs to be calibrated. The calibration is generally done in a static manner by measuring the anemometer output in a steady flow at various known velocities. A characteristic law is then deduced from these data, which is then used in a dynamic mode to measure instantaneous flow velocities.

In our experiments, the calibration is performed in the potential core of the jet where the velocity is quasi-uniform with a very low turbulence level. The reference velocity inside the potential core is estimated by a conventional pitot-static tube. The tube and the hot-wire were placed side by side with an adequate distance to avoid any influence of one instrument on the other. Velocity and voltage data have been recorded at 4096 Hz for 20 s at every velocity point. Figure 5.1 presents a photo showing the wire and the pitot tube placement. The velocity profile at the jet exit section has been measured with the pitot tube and because the output velocity is constant through the exit section (shown in figure 3.4a in section 3.5.2) and then the $\sim$ 1 cm distance between the hot wire and the pitot tube will not bias the data. This flat velocity profile was also measured with the hot wire anemometry to confirm this hypothesis (see section 3.5.2).

The pitot-static pressure difference has been recorded using a Huba Control differential pressure transmitter with a precision of $\pm 2$ Pa. Temperature of the flow was measured with a resolution of $\pm 0.001$°C. Using the Bernoulli equation, the pitot velocity is estimated from

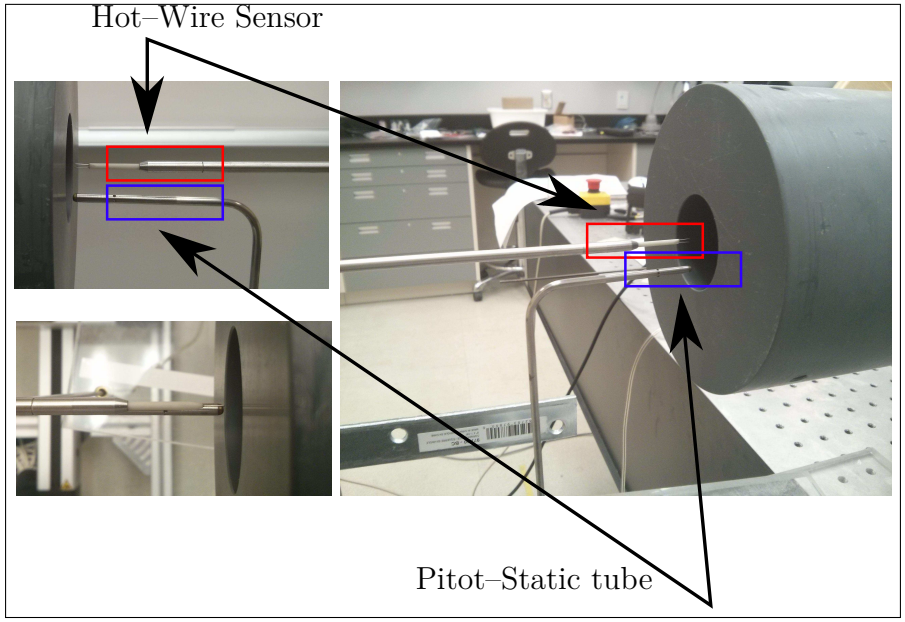


Figure 5.1: Positioning of the pitot-static tube and the hot-wire during the calibration procedure.

the pressure and temperature data by the following relation:

$$U = \sqrt{\frac{2\Delta P}{\rho}} \tag{5.1}$$

in which $\rho$ is the density of the flow (kg/m$^3$), $\Delta P$ the difference between the static and dynamic pressures (Pa) and $U$ is the velocity at the jet exit section (m/s).

In section 2.2, from the conservation of energy applied to a wire element we obtained the following equation relating the properties of the wire to that of the flow through the Nusselt number $Nu$:

$$R_w I_w^2 = \pi l \kappa (T_w - T_a) Nu. \tag{5.2}$$

The fundamental basis of the hot-wire anemometry depends primarily on the physical law that relates the heat transfer coefficient (represented by $Nu$) to the local flow velocity, or more exactly to the Reynolds number based on the wire characteristics:

$$Re_w = \frac{\rho U d}{\mu} \tag{5.3}$$

where $d$ is the wire diameter and $\mu$ the dynamic viscosity of air. Many empirical relations of $Nu = f(Re_w)$ can be found in the literature, and they will not be detailed here. These

relations can take different forms depending on the level of accuracy that we want to reach. One of the main disadvantages of our flow set-up is that the temperature can vary up to 10°C during a day, and this has a significant effect on the results. We therefore focused on the laws that incorporate temperature correction terms and after several tests, we finally chose to use the modified King law proposed by Collis and Williams (1959) which relates the Nusselt number to the Reynolds number for a circular wire placed normal to a flow:

$$Nu_f \left(\frac{T_f}{T_a}\right)^{-0.17} = A + BRe_w^{0.45}. \tag{5.4}$$

In this law, the calibration constants are $A$ and $B$, and the fluid characteristics are evaluated at the temperature $T_f$ of the hot fluid film that surrounds the wire, as sketched in figure 5.2. Collis and Williams proposed to define $T_f$ as the average temperature between the wire and the ambient fluid, *i.e.* $T_f = (T_w + T_a)/2$.

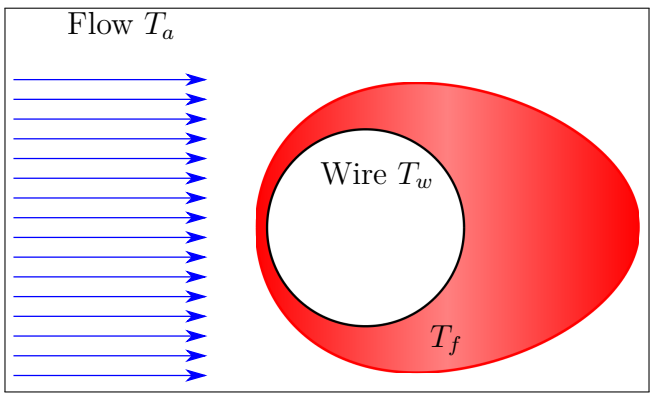


Figure 5.2: Thermal boundary layer developing on the wire.

With this law, equation 5.2 becomes:

$$\frac{R_w I_w^2}{\pi l \kappa_f (T_w - T_a)} \left(\frac{T_f}{T_a}\right)^{-0.17} = A + BRe_w^{0.45}, \tag{5.5}$$

in which all flow parameters have to be estimated at the film temperature $T_f$, indicated by the subscript $f$. The flow density dependence on the temperature $T$ is calculated using the ideal gas law for air at the ambient pressure $P_a$:

$$\rho(T) = \frac{P_a}{287.058 \times T}, \tag{5.6}$$

and the thermal conductivity and the dynamic viscosity using Sutherland's formula (Poling

*et al.*, 2001)

$$\mu(T) = \frac{1.4592 \times T^{3/2}}{109.10 + T}, \tag{5.7}$$

$$\kappa(T) = \frac{2.3340 \times 10^{-3} \times T^{3/2}}{164.54 + T}. \tag{5.8}$$

The constants $\pi$ and $l$ can be included in the calibration coefficients $A$ and $B$, and furthermore for a CTA anemometer the values of $R_w$ and $T_w$ are constant so that they can also be included in $A$ and $B$. Equation 5.5 therefore takes the final following forms:

$$\begin{aligned}
Q_1(T_w, T_a, R_w, I_w) &= A_1 + B_1 Re_w^{0.45} \qquad \text{for a CVA anemometer,} \\
A_1 &= A\pi l \\
B_1 &= B\pi l \\
Q_2(T_w, T_a, V_o) &= A_2 + B_2 Re_w^{0.45} \qquad \text{for a CTA anemometer,} \\
V_w &= I_w R_w \\
V_w &= C V_o \\
A_1 &= A\pi l R_w / C^2 \\
B_1 &= B\pi l R_w / C^2
\end{aligned}$$

which relate the flow velocity (through the Reynolds number) to the anemometer output variable $Q_1$ or $Q_2$. In the above equations $V_o$ is the CTA output voltage related to the wire voltage by a constant value C which is a different for each circuit.

Examples of calibration curves are presented in figure 5.3 for the CVA and the DISA anemometers. The linear relation between $Q_{i=1,2}$ and $Re_w^{0.45}$ is obtained with an excellent accuracy, which validates the use of the Collis and Williams calibration law to perform velocity measurements in our set-up.

Additional calibration curves are presented in figure 5.4 whose purpose is to analyze the repeatability of the calibration procedure. Results show that the calibration coefficients vary only slightly ($\sim 2\%$) from day to day. Therefore, the calibration was renewed every two days to guarantee a good accuracy for the estimation of turbulent quantities that are presented below.

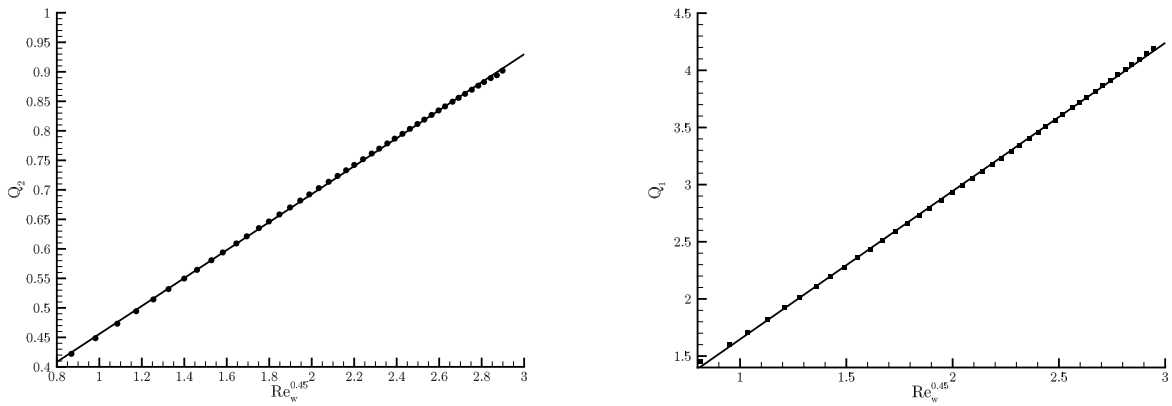


(a) CTA (DISA) calibration, $R^2 = 0.99980428$.

(b) CVA calibration, $R^2 = 0.99981059$.

Figure 5.3: Examples of two different calibration curves.

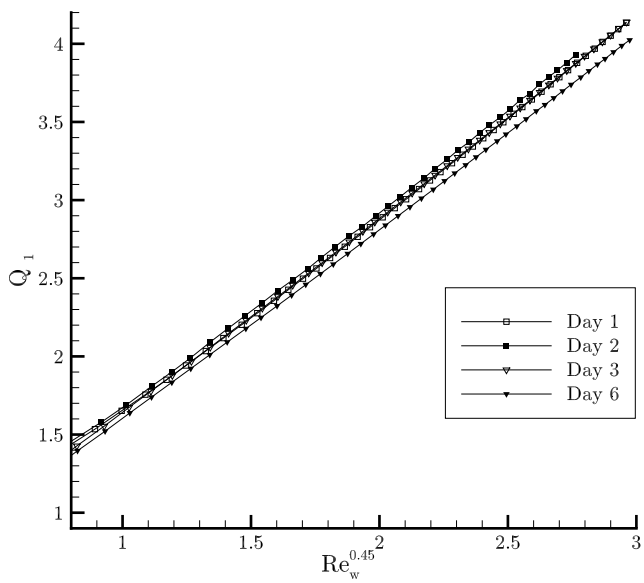


Figure 5.4: Test on the repeatability of the calibration procedure.

## 5.2 Mean and rms velocity profiles

The axisymmetric turbulent jet has been the subject of a considerable number of studies because of the various fundamental as well as practical interests (see, *e.g.*, Wygnanski and Fiedler, 1969; Panchapakesan and Lumley, 1993a,b; Hussein *et al.*, 1994; Malmstrom *et al.*,

1997; Fairweather and Hargrave, 2002; Falcone and Cataldo, 2003). The different regions that characterize the jet are schematically represented in figure 5.5 and are now briefly presented. We already know the existence of a potential core characterized by a uniform velocity and a low turbulence intensity (typically less than 1%), and where the hot-wires are calibrated. The potential core is bounded by a mixing layer that gradually develops in space from the nozzle lips to a downstream distance that marks the end of the potential core. Further downstream is a transition region where the flow redevelopment occurs. Depending on the Reynolds number, turbulence can appear at different axial positions. Here, the Reynolds number of the jet is sufficiently high to trigger turbulence a few diameters from the nozzle lips. As a consequence, a self-similar region should exist a few diameters behind the transition region, that is a region where the turbulent profiles present a similitude. In this region, we can expect that the turbulence is developed, which means that the power spectra of the velocity fluctuations should exhibit the well-known Kolmogorov law in the so-called inertial sub-range, *i.e.* a decrease in energy following $\sim f^{-5/3}$ where $f$ is the frequency.

Fluctuating velocity signals have been recorded in this region to validate the whole correction procedure required by the CVA system. This is because independently of the anemometer used, which delivers a voltage signal converted to a velocity signal through a calibration procedure, the real velocity fluctuation behaviour is physically known, at least in a frequency range, which presents an additional validation tool.

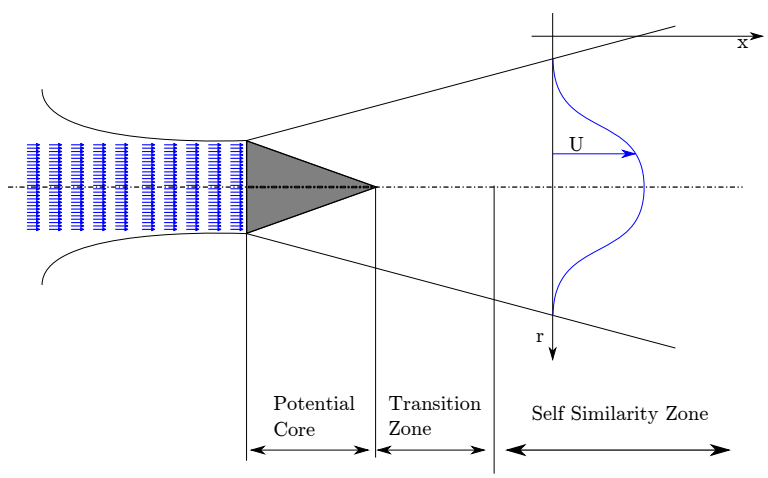


Figure 5.5: Zones of turbulent axisymmetric jet

Turbulent measurements were performed in the self-similar region of the jet at $x/D = 12$. Data have been recorded with both CTA and CVA anemometers using a National Instruments NI PXI-4495 DAQ card at a sampling rate of 204 800 Hz for 30 s. The Dantec Dynamics 5 µm 55P11 tungsten wire is operated with an overheat ratio of $\sim$ 0.6 yielding to a wire

temperature of $\sim$ 190°C with a resistance of 5.45 Ω. The same wire with the same connecting cable and support was also operated by the CVA anemometer with a voltage of $V_w = 0.550$ mV leading to an overheat ratio ranging from 0.6 to 1.14 depending on the flow velocity. Data were recorded using both available hardware compensations of the CVA system, *i.e.* with the TC1 and TC2 time constants. Since CTA and CVA signals cannot be recorded simultaneously, the spatial scanning of all measurement points was sequentially performed, first with the CTA, then with the CVA with the TC1 hardware compensation and finally with the TC2 hardware compensation. As a consequence, even if we tried to maintain the same flow conditions, the temperature can slightly differ between the recordings. Results are presented in figure 5.6 for non-compensated signals, *i.e.* without any software correction.

Uncertainty of the velocity data is the accumulated uncertainties of instrumentation, calibration, data acquisition and experimental conditions. Due to the relatively high cut-off frequency of the anemometers compared to the frequencies in the flow, the anemometer's frequency characteristics will not add to the uncertainty. The pitot-static tube used in calibration has relative standard uncertainty of $\pm 1\%$. The linearization of calibration curve (figure 5.3) has relative standard uncertainty of $\pm 0.22\%$. Data acquisition system having 24-bit resolution has relative standard uncertainty of less than $\pm 0.01\%$ which is assumed negligible. The same is true for temperature and pressure measurement uncertainties as well as humidity variations. The relative expanded uncertainty ($\epsilon_{tot}$) of the measured velocities is calculated as sum of all uncertainties of different sources ($\epsilon_i$).

$$\epsilon_{tot} = 2\sqrt{\sum \epsilon_i^2} = 2\sqrt{0.01^2 + 0.002^2} \simeq 0.0203 = 2.03\%. \tag{5.9}$$

This expanded uncertainty is shown with error bars in the figures 5.6 and 5.8.

The mean axial velocity profile is shown in figure 5.6a. The velocity is maximum ($\sim$ 20 m/s) on the jet axis and gradually decreases to zero as we move away from the axis. We can observe that the zero velocity is reached at a distance greater than 5 radii from the axis which reveals the considerable entrainment produced by the jet on the surrounding fluid. Results are very close for all anemometer systems (difference between 0.89% to 5.28% detailed in table 5.1), with a slight difference in the vicinity of the axis location and a more important discrepancy at the jet boundary. In this latter region, it is important to note that the hot-wire has not been calibrated for such low velocities as the minimum of $Re_w^{0.45}$ in figure 5.3 was 0.8 which corresponds to a minimum velocity of $\sim$ 1.9 m/s. However, at these low velocities the calibration requires special care because the heat conduction through the wire prongs is more important as well as the natural convection effects, so that generally the hot-wire anemometry is not used at low velocities. We will therefore analyze our results closer to the

jet axis.

More significant differences are observed in the rms profile presented in figure 5.6b. All curves show the same trend: $u_{\text{rms}}$ increases first as we move away from the axis, reach a maximum at $r/R \sim 1$ and then gradually decreases to zero as we approach the jet boundary, which is typical at this axial position and comes from the production of turbulence energy by the Reynolds stresses (see, *e.g.*, Hussein *et al.*, 1994). Again, measurements at the edge of the jet, where all results appear to be consistent, should not be considered since in this region the turbulence intensity can exceed 50% (which is no more a small perturbation), in contradiction with the assumption that the anemometer response to small perturbations is linear.

We consider CTA the ideal anemometer and expect that a single physical parameter (jet flow velocity) should be recorded the same regardless of using different instruments (CTA and CVA using either TC1 or TC2). The important discrepancies observed in the rms profile are however expected because the CVA signals are not yet compensated for the wire response whose cut-off frequency is far lower than that of the CTA system. This explain why differences are more pronounced on $u_{\text{rms}}$ than on $\overline{U}$. The effect of the software compensation will now be investigated, and we focus first on the velocity spectra.

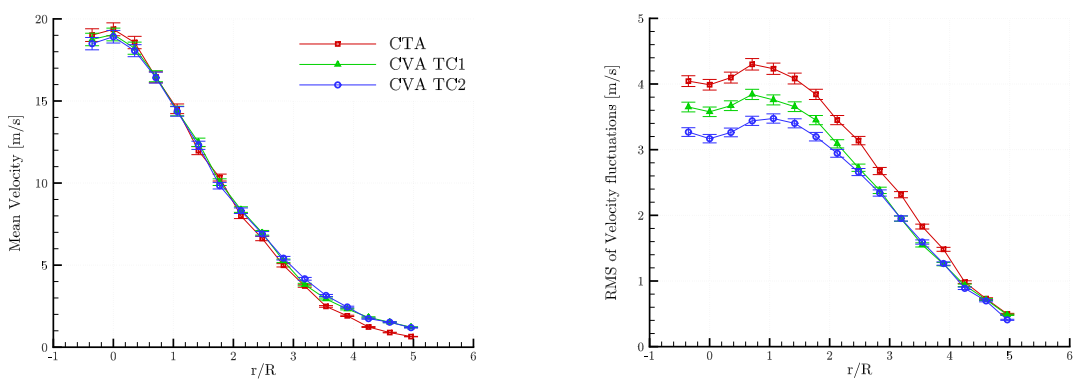


(a) Mean velocity $\overline{U}$

(b) Amplitude of velocity fluctuations $u_{\text{rms}}$

Figure 5.6: Radial turbulent profiles at $x/D = 12$.

## 5.3 Turbulent spectra

Now if we return to the results related to figure 5.6, figure 5.7 presents spectra of velocity fluctuations obtained on the jet axis ($x/D = 12$) for three radial positions. The shape of

the spectra is typical of the turbulent energy cascade. For each position, the CTA spectrum is shown with both non-corrected and corrected CVA spectra with the time constant $M_{\mathrm{CVA}}$ that was measured in section 4.3. As can be observed for the first position ($r/R = 0$, figure 5.7a), if non-corrected, spectra of signals modified with an hardware compensation have a lower amplitude than the reference CTA spectrum. This is particularly evident for the TC2 time constant for which the frequency from which fluctuations are amplified is much higher than the actual wire cut-off frequency, which results in an important difference in the spectra amplitudes that begins to appear at a frequency as low as $\sim$ 200 Hz. This is also the case for TC1 even if this difference is smaller. On the contrary, when the software correction is applied, both CVA signals agree with the CTA spectrum up to $\sim$ 40 kHz (figure 5.7). For higher frequencies, the CTA spectrum shows a bump that cannot by physical. This bump corresponds actually to the small amplification of the CTA transfer function that was studied in section B.3 (see figure B.7b). These results then show that the CVA anemometer can respond to higher frequencies than the CTA anemometer without signal deformation. Finally, the dashed line shown in the plot is the Kolmogorov law that predicts a power spectrum proportional to $f^{-5/3}$ for isotropic turbulence. The close agreement with the computed velocity spectra shows that a local isotropy is indeed observed starting from a particular frequency ($\simeq$ 200 Hz for the flow in the jet centre and $\simeq$ 80 Hz for the flow in the jet radii).

Figures 5.7b and 5.7c show similar characteristics on spectra obtained at two other locations. The discrepancy between the non-corrected TC1 spectrum and the CTA spectrum is more pronounced than previously seen on the jet axis but after correction, all spectra are perfectly superimposed [1]. The differences between spectra can be numerically represented if we look at the values of $u_{\mathrm{rms}}$ which will be presented in the next section.

## 5.4 Velocity profiles

We have seen that CVA velocity spectra can be significantly affected by the software correction, especially for the TC2 time constant. Since according to the Parseval theorem the energy of a signal $\overline{u'^2(t)}$ equals the integration of the power spectrum of this signal over the full frequency range, $u_{\mathrm{rms}}$ should be affected. Figure 5.8 shows the effect of the software correction on the mean velocity (figure 5.8a) and on the rms level (figure 5.8b). While the effect

[1] You can note that an important noise is present in velocity signals. This noise is in fact produced by the controller of the travel axis that is used to automatically move the probe in order to generate profiles easier and faster than manually. When the power controller is off, most of the noise is removed and spectra are similar to the ones shown in figure C.9. However, by doing this, the reference of the coordinate system is lost so that we chose to perform measurement with the controller power on

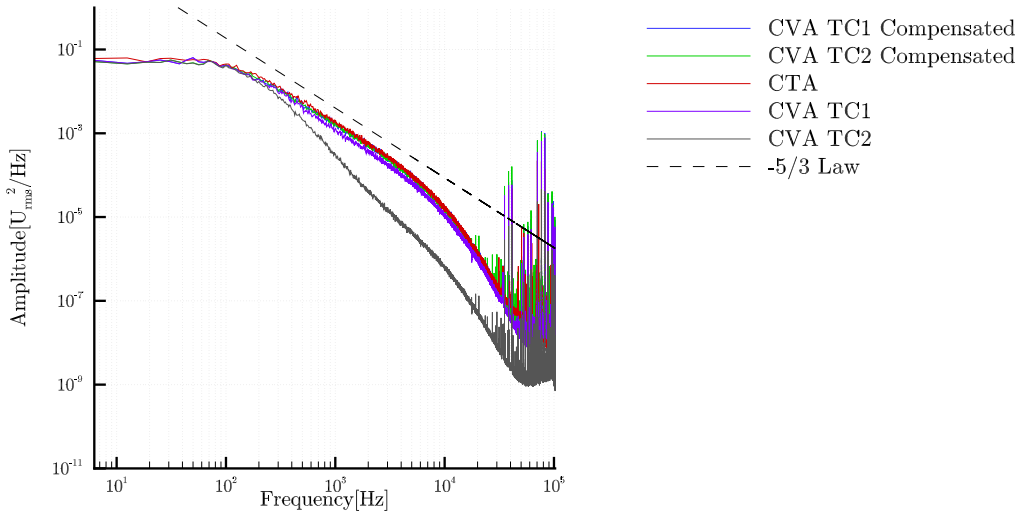


(a) $r/R = 0$

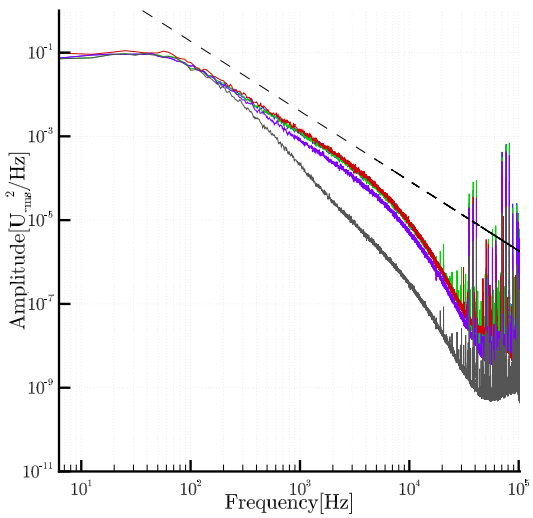


(b) $r/R = 1$

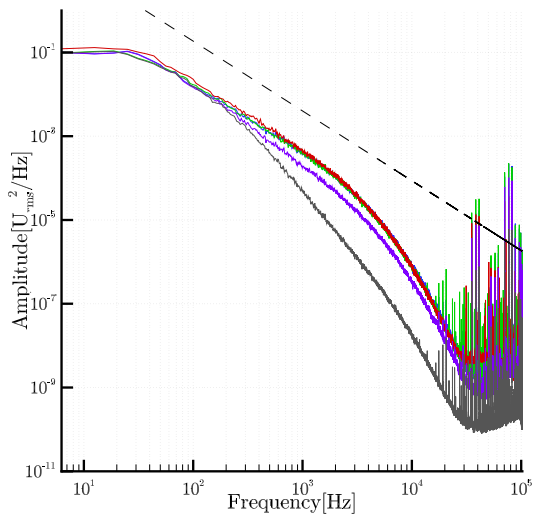


(c) $r/R = 2.5$

Figure 5.7: Power spectra of velocity fluctuations at $x/D = 12$.

on the mean values are negligible, the corrected rms values are significantly altered since the loss of energy in the signal due to the wire frequency response is recovered, and a better match with the CTA values is obtained. Corrections for $r/R > 2.5$ have not been performed because the $M_{\mathrm{CVA}}$ calibration was not obtained for the corresponding mean velocities that are relatively low. An extrapolation could have been done but as already stated, this range

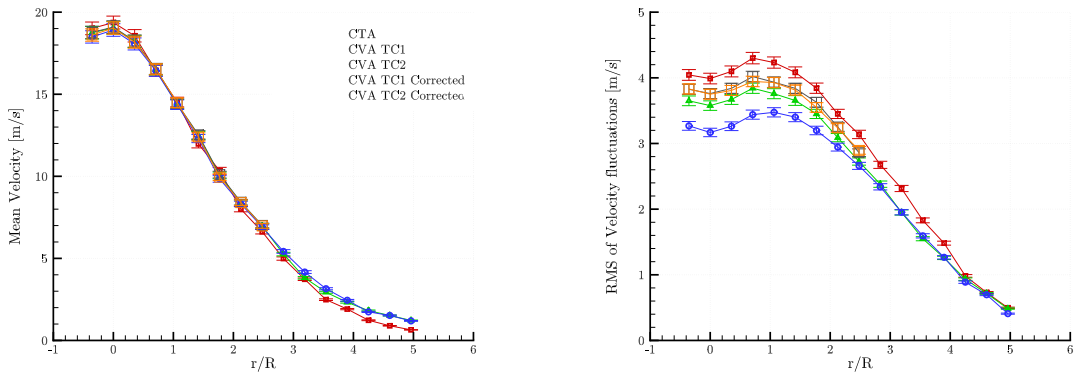


(a) Mean velocity $\overline{U}$ (b) Amplitude of velocity fluctuations $u_{\text{rms}}$

Figure 5.8: Radial turbulent profiles at $x/D = 12$

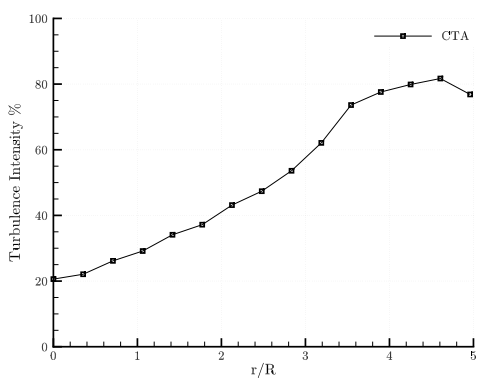


Figure 5.9: Turbulent intensity profiles at $x/D = 12$

of velocities is not considered in this study.

The exact values for the three locations for which we analyzed the spectra are gathered in table 5.1 for the mean velocities and table 5.2 for the rms. At high velocities (jet centre,$r/R = 0$) the mean values differ by only $\sim 1\%$, but the rms values show a discrepancy $\sim 7\%$, which is not negligible.

Several factors can explain the difference between the CTA and the CVA measurements. Since CTA rms values are always greater than CVA values, one possible reason is that the CTA anemometer amplifies a frequency range due to its frequency response that is not perfectly flat before the cut-off frequency (see figure B.7b). However, even if this amplification was corrected, the rms values should be only slightly affected. We can also note that mean

Table 5.1: Influence of the software correction on the mean velocity values (m/s).

| Position | CTA | TC1 | TC1 corr. | TC1 vs CTA | TC1 corr. vs CTA |
|---|---|---|---|---|---|
| $x/R = 0$ | 19.37 | 19.05 | 19.09 | -1.65% | -1.44% |
| $x/R = 1$ | 14.52 | 14.39 | 14.43 | -0.89% | -0.62% |
| $x/R = 2.5$ | 6.62 | 6.97 | 7.01 | +5.28% | +5.89% |

| Position | CTA | TC2 | TC2 corr. | TC2 vs CTA | TC2 corr. vs CTA |
|---|---|---|---|---|---|
| $x/R = 0$ | 19.37 | 18.91 | 19.03 | -2.37% | -1.75% |
| $x/R = 1$ | 14.52 | 14.36 | 14.48 | -1.10% | -0.27% |
| $x/R = 2.5$ | 6.62 | 6.90 | 6.97 | +4.23% | +5.29% |

Table 5.2: Influence of the software correction on the rms velocity values (m/s).

| Position | CTA | TC1 | TC1 corr. | TC1 vs CTA | TC1 corr. vs CTA |
|---|---|---|---|---|---|
| $x/R = 0$ | 3.99 | 3.58 | 3.76 | -10.28% | -5.76% |
| $x/R = 1$ | 4.23 | 3.76 | 3.93 | -11.11% | -7.09% |
| $x/R = 2.5$ | 3.14 | 2.72 | 2.86 | -13.38% | -8.92% |

| Position | CTA | TC2 | TC2 corr. | TC2 vs CTA | TC2 corr. vs CTA |
|---|---|---|---|---|---|
| $x/R = 0$ | 3.99 | 3.17 | 3.75 | -20.55% | -6.01% |
| $x/R = 1$ | 4.23 | 3.47 | 3.93 | -17.97% | -7.09% |
| $x/R = 2.5$ | 3.14 | 2.66 | 2.89 | -15.29% | -7.96% |

and rms values are very close for different TC time constant, which is consistent.

However, the main reason why the CVA does not respond as the CTA is probably that the constant voltage anemometer is more sensitive to non-linear effects (Berson *et al.*, 2009). This is related to the fact that the cut-off frequency of the CVA, without partial hardware compensation, is close to that of the wire, *i.e.* a few hundreds of Hz, and the correction is performed as a post-processing treatment. From results shown in figure 5.9, we can note that turbulence intensity is between 20 and 50% which is very high. The good news is that an additional correction can be performed to compensate for non-linear effects (Berson *et al.*, 2009).

# Chapter 6
# Conclusion

In this work, the constant voltage anemometer has been studied in detail. This system is manufactured by only one company and as a consequence is largely less common than the constant temperature anemometer that is used in most of experimental research and industrial laboratories all over the world. To date, a robust procedure to perform accurate CVA measurements is still lacking, and CVA signals have never been compared to another technique to analyze its frequency response. This was the primary objectives of this study.

A CVA measurement is not easy to implement as it requires special precautions that are not always easy to fulfill. First, since the working principle is based on a constraint on the wire voltage and not on the wire temperature, the wire time constant is not constant but varies with the velocity, and needs to be measured. A calibration of the wire time constant $M_{\mathrm{CVA}}$ can however be done in conjunction with the calibration of the wire that will provide the relation between the output voltage of the anemometer and the flow velocity. Even if the wire time constant is sensitive to many flow parameters, we have calculated that the corrected rms velocity values are not affected more than $\pm$ 1.1% (compared to CTA) if the time constant is modified by $\pm$ 5%, which means that a rough estimate can, at worst, be used.

The wire response is corrected through a software compensation that can be performed either in the temporal domain or in the Fourier space. Since this is a post-treatment, the real response of the CVA system should be close to the wire response which is due to its thermal inertia, and that can be considered as a first-order system. As a consequence, the cut-off frequency reach only a few hundred hertz, which is not sufficient for turbulent flows. To compensate for this and to improve the signal to noise ratio, the CVA anemometer is provided with an additional RC electronic circuit that amplifies the signal above a fixed frequency, corresponding to a fixed time constant. By properly estimating this time constant, we came to the conclusion that the values given by the manufacturer are not accurate. This could come from electronic components of low quality or a different behavior of the RC circuit when connected to the CVA. Nevertheless, we have described a method that allows to confirm that the circuit indeed acts as a first order system and then we have deduced the right values that have been confirmed by measurements. The CVA anemometer in known to be able to obtain instantness in situ cold wire resistance ($R_a$). However we showed that the so called PDR method used to obtain $R_a$ is not reliable and should not be implemented in sensitive measurements, where an accurate value of $R_a$ is required.

Knowing the wire time constant $M_{\mathrm{CVA}}$ as well as the amplifier time constant (TC1 or

TC2), a software correction is finally performed to remove the effect of the electronic amplifier and to correct for the wire thermal inertia. To validate the whole methodology, velocity measurements have been performed in a round turbulent jet and compared to the more standard constant temperature anemometer. An excellent agreement is obtained on the spectral response of the CVA and CTA systems, except that at highest frequencies ($\sim$ 50 kHz) the CTA response is altered. This response can be tuned but at these frequencies this is not easy and stable. On the contrary, the CVA system can reach higher frequencies without any problem. As a consequence, the CVA appears as a very promising technique in supersonic flows where turbulent fluctuations can reach frequency of the order of megahertz.

However, it is probable that the CVA system underestimates the root-mean-square values of turbulent velocity fluctuations. It is known that a simple tuning of the time constant of a CTA system is probably not sufficient. For this reason to obtain accurate measurements a correction should be performed to compensate for the transfer function that is not rigorously flat before the cut-off frequency. According to the results presented in this work, the problem should come from nonlinearities to which the CVA anemometer is known to be very sensitive, or at least more sensitive than the CTA anemometer. While it is possible to correct voltage signals to consider the effect of such non-linearities, it appears that to treat this problem the turbulent jet is not the best choice. The reason being as we move away from the jet axis, the turbulence decreases less rapidly than the mean velocity to that the local turbulence intensity can reach very high values. Even in the jet center, we measured levels as high as 20%. This is why in some studies the flying hot-wire technique (consisting in performing measurements with a probe moving with a constant speed) was used to increase the velocity seen by the wire and then to decrease the turbulence intensity. However, such a technique is not easy to implement and has a considerable number of constraints.

An alternative would be to apply the CVA technique to a turbulent boundary layer. As we move from the surface, the turbulence intensity also decreases but on the contrary the mean velocity increases, thus eliminating the problem of non-linearities. Furthermore, the boundary layer profile of mean and fluctuating velocities is theoretically known for a zero-pressure gradient, along with the frequency content through the Kolmogorov law, which represents an ideal test case with a high level of validation for the constant voltage anemometry.

The conclusions of this research can be summarized as follows:

- Internal calibration of CVA anemometer is done, measuring values of coefficients "a" and "b" (relating wire resistance to output voltage) and internal amplifiers time constant (TC1 and TC2)

- Measurement of wire cold resistance using known PDR method with CVA system is

not reliable

- Wire time constant $M_{\mathrm{CVA}}$ is measured accurately and it has been calibrated with flow velocity and temperature changes
- Frequency response of CTA anemometer is measured
- The spectrum of velocity measured with CVA and CTA system are superimposed after implementing time constant compensation on the CVA data
- The CVA system yet under estimate root mean square values of the velocity compared to CTA system

# Bibliography


BARRE, S., DUPONT, P. and DUSSAUGE, J. (1992). Hot-Wire measurements in turbulent transonic-flows. *European Journal of Mechanics B-Fluids*, 11, 439–454.

BELL, J. H. and MEHTA, R. D. (1988). Contraction design for small low-speed wind tunnels. *NASA STI/Recon Technical Report N*, 89, 13753.

BERSON, A., BLANC-BENON, P. and COMTE-BELLOT, G. (2009). A strategy to eliminate all nonlinear effects in constant-voltage hot-wire anemometry. *Rev Sci Instrum*, 80, 045102. Doi: 10.1063/1.3103948.

BERSON, A., POIGNAND, G., BLANC-BENON, P. and COMTE-BELLOT, G. (2010a). Capture of instantaneous temperature in oscillating flows: use of constant-voltage anemometry to correct the thermal lag of cold wires operated by constant-current anemometry. *Rev Sci Instrum*, 81, 015102. Doi: 10.1063/1.3274155.

BERSON, A., POIGNAND, G., BLANC-BENON, P., COMTE-BELLOT, G. and ASME (2010b). A new procedure to capture temperature fluctuations using cold wires: application to thermoacoustic systems. *Proceedings of the Asme Fluids Engineering Division Summer Conference - 2010, Vol 2*, 97–103.

BLANCHARD, A., LACHOWICZ, J. and WILKINSON, S. (1997). NASA Langley Mach 6 quiet wind-tunnel performance. *AIAA JOURNAL*, 35, 23–28. AIAA 34th Aerospace Sciences Meeting and Exhibit, RENO, NV, JAN 15-19, 1996.

BRUUN, H. (1995). *Hot-Wire anemometry: principles and signal analysis*. Oxford University Press.

COLLIS, D. and WILLIAMS, M. (1959). Two-dimensional convection from heated wires at low reynolds numbers. *Journal of Fluid Mechanics*, 6, 357–384.

COMTE-BELLOT, G. (1976). Hot-wire anemometry. *Annual review of fluid mechanics*, 8, 209–231.

COMTE-BELLOT, G. and SARMA, G. R. (2001). Constant voltage anemometer practice in supersonic flows. *AIAA journal*, 39, 261–270.

COMTE-BELLOT, G., WEISS, J. and BÉRA, J.-C. (2004). Lead-resistance effects in a constant voltage anemometer. *Review of Scientific Instruments*, 75, 2075.

FAIRWEATHER, M. and HARGRAVE, G. (2002). Experimental investigation of an axisymmetric, impinging turbulent jet. 1. velocity field. *Experiments in Fluids*, 33, 464–471.

FALCONE, A. M. and CATALDO, J. C. (2003). Entrainment velocity in an axisymmetric turbulent jet. *Journal of Fluids Engineering*, 125, 620.

FREYMUTH, P. (1967). Feedback control theory for constant-temperature hot-wire anemometers. *Review of Scientific Instruments*, 38, 677.

HAN, Y. O., GEORGE, W. K. and HJARNE, J. (2005). Effect of a contraction on turbulence. part 1: Experiment. *43rd AIAA Aerospace Sciences Meeting and Exhibit, January 10, 2005 - January 13, 2005*. American Institute of Aeronautics and Astronautics Inc., 43rd AIAA Aerospace Sciences Meeting and Exhibit - Meeting Papers, 4241–4252.

HANCOCK, P. and JOHNSON, A. (1997). Close spacing of settling chamber screens. *Aeronautical Journal*, 101, 179–183.

HULTMARK, M. and SMITS, A. J. (2010). Temperature corrections for constant temperature and constant current hot-wire anemometers. *Measurement Science and Technology*, 21, 105404.

HUSSEIN, H. J., CAPP, S. P. and GEORGE, W. K. (1994). Velocity measurements in a high-reynolds-number, momentum-conserving, axisymmetric, turbulent jet. *Journal of Fluid Mechanics*, 258, 31–75.

KEGERISE, M. and SPINA, E. (2000). A comparative study of constant-voltage and constant-temperature hot-wire anemometers part i: The static response. *Experiments in fluids*, 29, 154–164.

MALMSTROM, T. G., KIRKPATRICK, A. T., CHRISTENSEN, B. and KNAPPMILLER, K. D. (1997). Centreline velocity decay measurements in low-velocity axisymmetric jets. *Journal of Fluid Mechanics*, 346, 363–377.

MANGALAM, S. M. (2004). Real-time extraction of hydrodynamic flow characteristics using surface signatures. *Oceanic Engineering, IEEE Journal of*, 29, 622–630.

MCKEON, B. J., COMTE-BELLOT, G., FOSS, J. F., WESTERWEEL, J., SCARANO, F., TROPEA, C., MEYERS, J. F., LEE, J. W., CAVONE, A. A., SCHODL, R., KOOCHESFAHANI, M. M., NOCERA, D. G., ANDREOPOULOS, Y., DAHM, W. J., MULLIN, J. A., WALLACE, J. M., VUKOSLAVČEVIĆ, P. V., MORRIS, S. C., PARDYJAK, E. R. and

CUERVA, A. (2007). Velocity, vorticity, and mach number. C. Tropea, A. L. Yarin and J. F. Foss, editors, *Springer handbook of experimental fluid mechanics*, Springer, volume 1.

MIKHAILOVA, N., REPIK, E. and SOSEDKO, Y. P. (1994). Optimal control of free-stream turbulence intensity by means of honeycombs. *Fluid dynamics*, 29, 429–437.

MOREL, T. (1975). Comprehensive design of axisymmetric wind tunnel contractions. *Journal of Fluids Engineering*, 97, 225–233.

PANCHAPAKESAN, N. and LUMLEY, J. (1993a). Turbulence measurements in axisymmetric jets of air and helium. part 1. air jet. *Journal of Fluid Mechanics*, 246, 197–223.

PANCHAPAKESAN, N. and LUMLEY, J. (1993b). Turbulence measurements in axisymmetric jets of air and helium. part 2. helium jet. *Journal of Fluid Mechanics*, 246, 225–247.

POLING, B. E., PRAUSNITZ, J. M., JOHN PAUL, O. and REID, R. C. (2001). *The properties of gases and liquids*, volume 5. McGraw-Hill New York.

SARMA, G. (1991). Flow rate measuring apparatus. *US Patent*, 5074147.

SARMA, G. R. (1998). Transfer function analysis of the constant voltage anemometer. *Review of Scientific Instruments*, 69, 2385.

SARMA, G. R. and COMTE-BELLOT, G. (2002). Automated constant voltage anemometer for measurements with fluid temperature drifts. *Review of Scientific Instruments*, 73, 1313.

SARMA, G. R., COMTE-BELLOT, G. and FAURE, T. M. (1998). Software corrected hot wire thermal lag for the constant voltage anemometer featuring a constant bandwidth at the selected compensation setting. *Review of Scientific Instruments*, 69, 3223.

SCHEIMAN, J. and BROOKS, J. (1981). Comparison of experimental and theoretical turbulence reduction from screens, honeycomb, and honeycomb-screen combinations. *Journal of Aircraft*, 18, 638–643.

TAN-ATICHAT, J. (1980). *Effects of axisymmetric contractions on turbulence of various scales*. Illinois Institute of Technology.

TAN-ATICHAT, J., NAGIB, H. and LOEHRKE, R. (1982). Interaction of free-stream turbulence with screens and grids: a balance between turbulence scales. *Journal of Fluid Mechanics*, 114, 501–528.

TRUZZI, G. E., SARMA, G. R. and CHOKANI, N. (2002). Constant voltage anemometer operated hot wire at subsonic speeds over wide overheats in unsteady flows. *Review of Scientific Instruments*, 73, 4363.

WEISS, J., KNAUSS, H. and WAGNER, S. (2001). Method for the determination of frequency response and signal to noise ratio for constant-temperature hot-wire anemometers. *Review of Scientific Instruments*, 72, 1904.

WEISS, J. L., CHOKANI, N. and COMTE-BELLOT, G. (2005). Constant-temperature and constant-voltage anemometer use in a Mach 2.5 flow. *AIAA journal*, 43, 1140–1143.

WYGNANSKI, I. and FIEDLER, H. (1969). Some measurements in the self-preserving jet. *Journal of Fluid Mechanics*, 38, 577–612.

# Governing equations of CVA

The governing equations for constant voltage anemometry are driven as represented in Sarma (1998). For the basic CVA circuit with no compensation (as seen in figure A.1), the voltage across the hot wire is given by

$$V_w = \frac{R_F}{R_1} V_1 \tag{A.1}$$

and the output voltage $V_s$ of the basic circuit can be expressed as

$$V_s = \frac{V_1}{R_1}\left[R_g + R_h + R_F + \frac{(R_g + R_h)R_F}{R_w + r_L}\right]. \tag{A.2}$$

Defining

$$R_2 = R_g + R_h \tag{A.3}$$

and using equation A.1 it can be said

$$V_s = V_w\left[1 + \frac{R_2}{R_F} + \frac{R_2}{R_w + r_L}\right] \tag{A.4}$$

$$\begin{aligned}
\frac{V_s}{V_w} &= \left[1 + \frac{R_2}{R_F} + \frac{R_2}{R_w + r_L}\right] \\
\frac{V_s}{V_w} - \left(1 + \frac{R_2}{R_F}\right) &= \frac{R_2}{R_w + r_L} \\
\frac{1}{R_w + r_L} &= \frac{V_s}{V_w}\frac{1}{R_2} - \left(\frac{1}{R_2} + \frac{1}{R_F}\right) \\
R_w + r_L &= \frac{1}{\frac{1}{R_2}\frac{V_s}{V_w} - \left(\frac{1}{R_2} + \frac{1}{R_F}\right)} && \text{(A.5)} \\
R_w + r_L &= \frac{1}{a\frac{V_s}{V_w} + b} && \text{(A.6)}
\end{aligned}$$

where the coefficients a and b are usually defined through internal calibration, as explained in section 4.

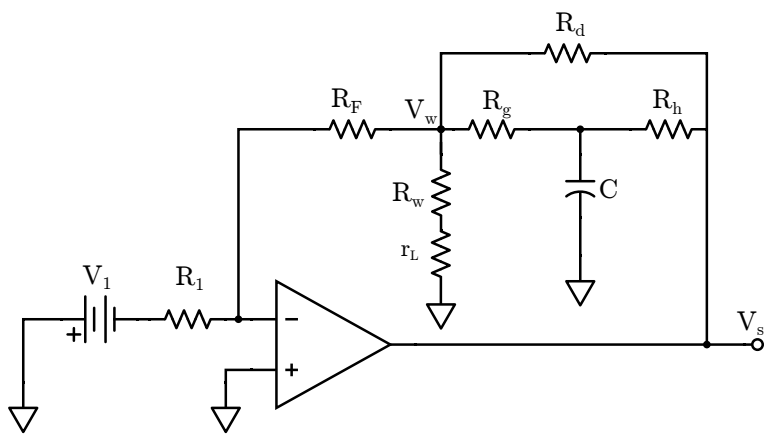


Figure A.1: Electronic circuit of the CVA anemometer ($R_w$: sensing wire).

# The frequency response of the constant temperature anemometer

We have studied the frequency response of the CVA system and the thermal lag of the wire, and we also suggested that by applying hardware and software compensations the output voltages of the CVA anemometer can be reliable. A final treatment has to be performed to recover the signal that is the closest to the true velocity signal by compensating for the time constant of the wire, however we need a reference velocity signal to compare with. The CTA anemometer is the only choice, particularly because the working principle is different from that of the CVA, but these systems have also their own frequency response and limits, which is the focus of this chapter.

## B.1 General Procedure

In the CTA systems the amplifier gain, offset voltage and compensating reactance can be adjusted accordingly to achieve the desired frequency response of the circuit and the wire together. Thus the wire thermal lag will be always compensated by the adjusted hardware without any need for a software compensation. This can be done because contrary to the CVA circuit, in the CTA working principle the resistance and the overheat of the wire are maintained constant, which means that the wire time constant depends only on the velocity, but only slightly. This simplicity in optimizing the circuit is one of the advantages of the CTA over the CVA anemometer.

The effect of the circuit adjustment on the frequency response of a CTA has been studied by Weiss *et al.* (2001). Based on earlier studies they suggested that in the usual frequency range the transfer function $H_B$ of the Wheatstone bridge (including the wire response) can be obtained by injecting a prescribed intensity perturbation through an electrical circuit connected in parallel of the wire and its connector, thus simulating a known velocity perturbation as already seen in section 4.3. In these conditions $H_B$ can be approximated as the product of the transfer function of the injecting signal $H_E$ with the transfer function of the wire through the following equation:

$$H_B(s) \approx \frac{K_1}{s\tau + 1} H_E(s), \tag{B.7}$$

where $s$ is the variable of the Laplace transform, $\tau$ the time constant of the wire (same concept as $M_{\mathrm{CVA}}$ as explained in the previous chapter) and $K_1$ a constant value. If a unit step (whose Laplace transform is $1/s$) is chosen as the injected perturbation, the transfer

function can be further simplified. By replacing $s$ by $j\omega$, we obtain:

$$H_B(\omega) \approx K_1 \frac{j\omega}{j\omega\tau + 1} \mathscr{F}[e_0(t)] \tag{B.8}$$

where $\mathscr{F}$ is the operator of the Fourier transform and $e_0(t)$ is the response of the bridge to the input signal. Finally, for frequencies above the wire thermal cut–off frequency ($\omega \gg 1/\tau$), we obtain:

$$H_B(j\omega) \approx \frac{K_1}{\tau} \mathscr{F}[e_0(t)] \tag{B.9}$$

so that for frequencies higher than the wire response, the transfer function of the CTA system can be approximately deduced from the Fourier transform of the response of the bridge to a step voltage. This procedure is now applied to a CTA that we have in our laboratory, the so called miniCTA.

## B.2 Frequency response of the MiniCTA anemometer

The 54N80 MiniCTA is a low-cost miniature CTA anemometer commercialized by Dantec Dynamics. It is dedicated for basic measurements of simple flows with moderate velocities and limited frequency content. We decided as a first choice to use this anemometer conjointly with the CVA system to make comparisons, but the disadvantages of this basic system is that we cannot perform any hardware adjustment, and moreover its frequency response is not provided by the manufacturer. The technique described above was therefore applied.

The wire was placed in the potential core of the jet and a step input in voltage was injected in the anemometer through the additional circuit presented in figure B.2. Using an Agilent Technologies 33521A waveform generator, different voltage amplitudes were fed to the system through a 1 k$\Omega$ resistance, and the output signal $e_0(t)$ was recorded by a National Instruments PXI-5922 24-Bit Flexible-Resolution Digitizer acquisition card at a sampling rate of 15 MHz. In order to repeat the process several times, a square signal was injected and the response of the MiniCTA was recorded during $\sim$ 20 periods to perform phase averaging. Finally, the Fourier transform of the signal was computed.

CTA responses for various step signal amplitudes are shown in figure B.3. To simulate a typical velocity step, a value of the input voltage signal should be around 30 mV. Independently of the step height, the response of the CTA is quite similar to a damped oscillating signal. However, a well-adjusted system should have a high damping so that a very few oscillations should be present (for example the system which will be studied in next section). Here, several oscillations (with $\simeq$0.1 ms period equivalent to 10 kHz) are clearly observed which probably means that the system is not correctly adjusted, a consequence of

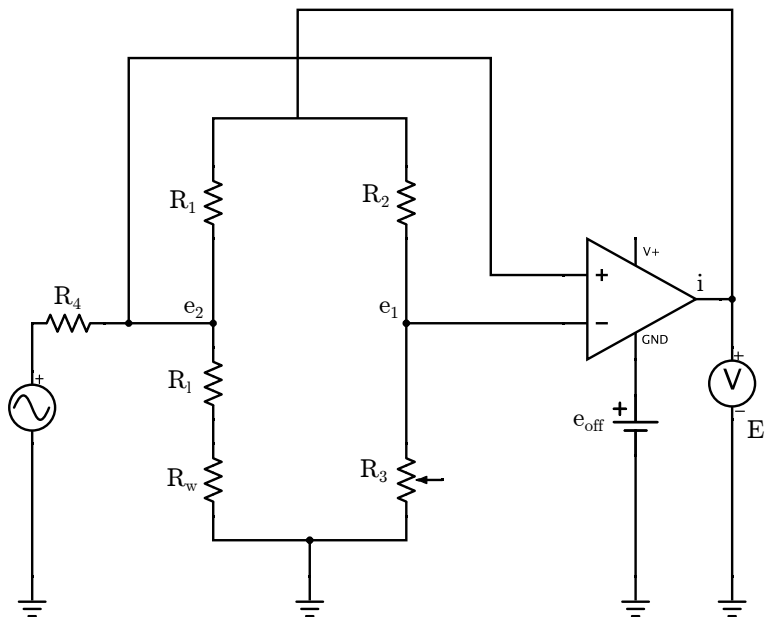


Figure B.2: The circuit of the CTA anemometer with the square wave injection

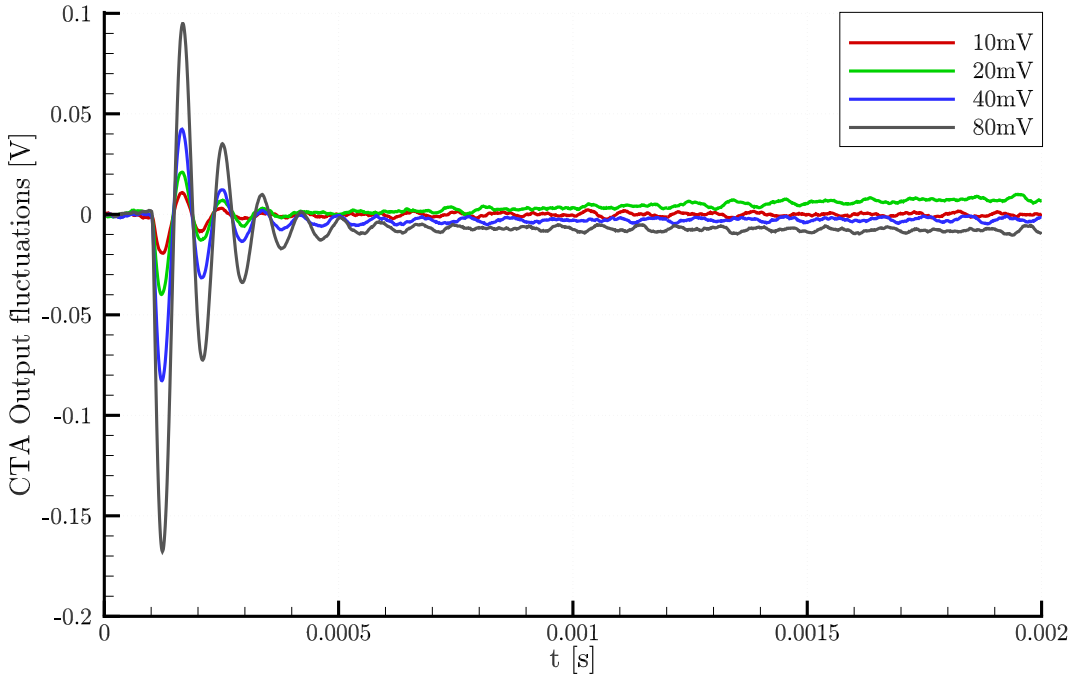


Figure B.3: Response of the MiniCTA anemometer to a step signal.

the fact that no hardware adjustments are possible and therefore, the frequency response of the anemometer cannot be properly adjusted. This phenomenon is still present even if we decrease the voltage to a value as low as 10 mV, for which the background noise, generated by the free-stream turbulence, is more apparent. On the contrary, if we increase the voltage, the number of detectable oscillations increase. We can not tell by looking at the time domain signal whether low amplitude step response and high amplitude step response have the same number of peaks or not. The peaks in low amplitude step response are in the same level as flow perturbations and would be difficult to detect. For this reason analysing the transfer function of these responses in frequency domain would be a solution.

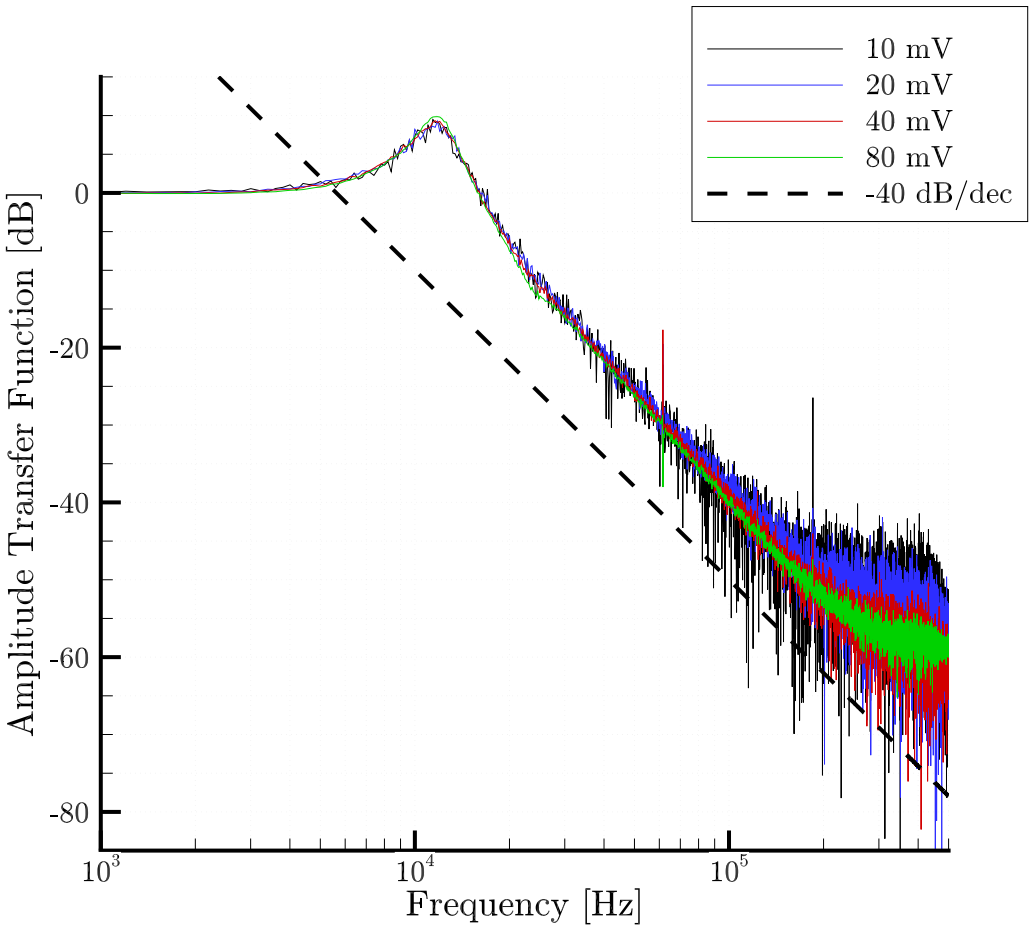


Figure B.4: Transfer function of the MiniCTA anemometer deduced from the square wave test.

The frequency responses, corresponding to signals shown in figure B.3, are presented in

figure B.4. A good response generally presents a gain as constant as possible until a cut-off frequency, followed by a gradual decay of the gain as the frequency increases. This is what we globally observed here, but in addition, since the frequency response corresponds to the Fourier transform of the temporal signals, the presence of oscillations in time results in an amplification of frequencies around the frequency of these oscillations. This is clearly observed in all the transfer functions shown in figure B.4, but the amplification is very important, of the order of $\sim$ 10 dB, which means that the resulting correction that we should apply to recover the original signal would be probably too important to be accurate.

Another argument that supports this conclusion can be deduced from figure B.5 that compares the temporal response for a positive (figure B.5a) and a negative (figure B.5b) step of 80 mV in amplitude. For a linear system, the response to a rising step is minus that of the falling step, but here we can note that the two responses are not similar, which emphasizes than the response is non-linear. This is indeed a behaviour that is observed when hardware adjustments are not perfect (Weiss *et al.*, 2001), and as a consequence, the MiniCTA was finally not found to be a good choice to provide reliable reference velocity signals, the system being more adapted to low frequency fluctuations. Another anemometer, the DISA system, was therefore explored.

## B.3 Frequency response of the DISA anemometer

The DISA 55M10 anemometer was designed by Dantec Dynamics several decades ago and is no longer available today. However, this anemometer is still used in research laboratories that specifically require very accurate data. Such a system is available at ÉTS and was therefore borrowed from Prof. J. Weiss in order to perform tests on our experimental set-up. The system allows to perform several adjustment, including the tuning of the time constant of the frequency response via an on-board circuit that injects a square wave signal through the wire. This is achieved once the wire is placed in a low-turbulent region of a flow, and the response is analyzed analogically on an oscilloscope.

A typical response of a CTA system to a square wave input voltage is presented in figure B.6. Bruun (1995) shows that if the anemometer behaves as a second-order system, the time constant $\tau$ can be obtained by estimating the width of the pulse from its start to when it drops to 97% of its maximum value, and the corresponding cut-off frequency is given by $f_c = 1/(1.3\tau)$. The response of the DISA anemometer was tuned manually with two potentiometers and the results are shown in figure B.7. In figure B.7a, we can observe that the temporal response contains almost no oscillations indicating that the adjustment is correct. The time constant that can be calculated predicts that the cut-off frequency of the system is $f_c \simeq 100$ kHz. This is confirmed in the transfer function (the Fourier transform of

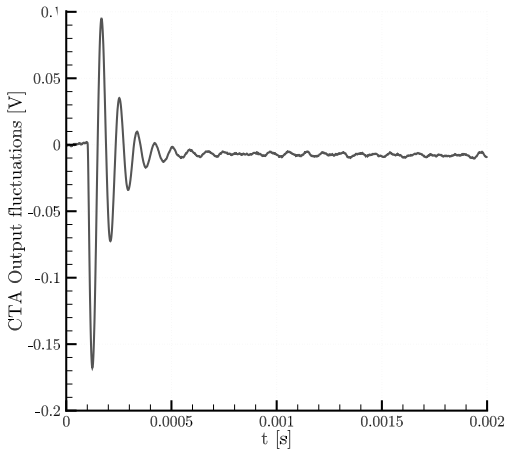


(a) Response to a rising step voltage

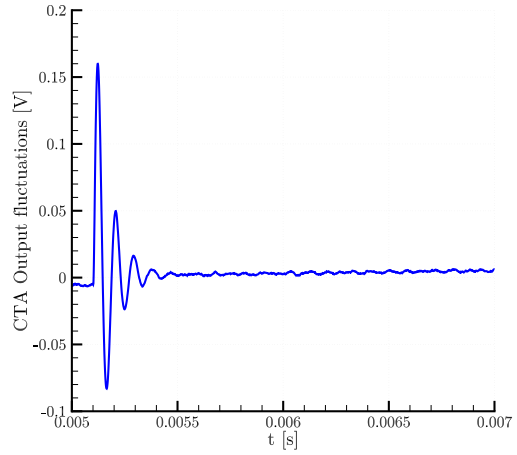


(b) Response to a falling step voltage

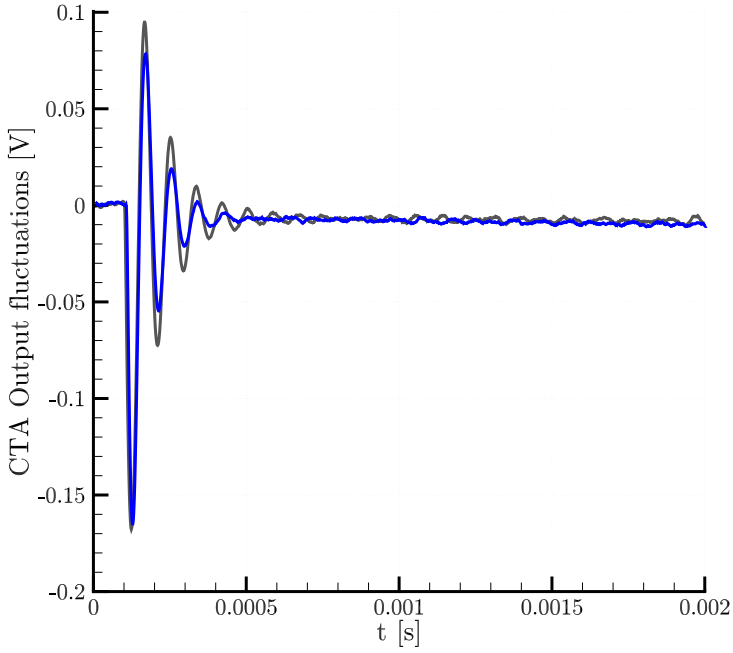


(c) Plot b flipped and placed over plot a to compare oscillations

Figure B.5: Response of the MiniCTA anemometer to a 80 mV step signal.

the temporal response of one step input) shown in figure B.7b where a slight increase of the gain is observed around this frequency, however the increase is very low ($\sim$ 1 dB) compared to the MiniCTA, a consequence of the quasi-absence of oscillations in the temporal response.

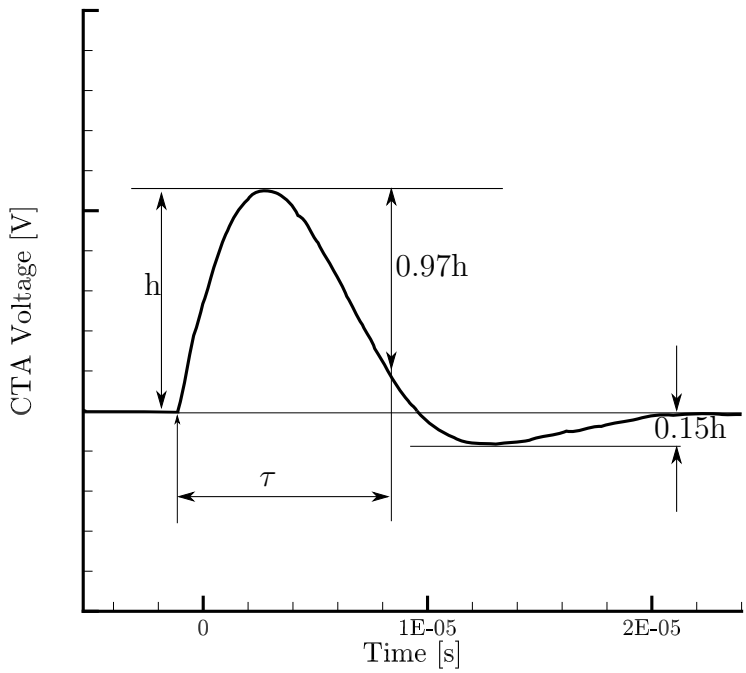


Figure B.6: Example of an ideal response of a well-adjusted CTA system to a square-wave test (adapted from Freymuth (1967); Bruun (1995)).

The analyzing of the DISA CTA transfer function performed here shows that the frequency response of the system is flat to within 1 dB up to $f_c \simeq 100$ kHz. This is close to the maximum frequencies that will be investigated in this work so that it was decided to consider the signals delivered by the DISA anemometer as reference signals and no corrections were applied to these signals.

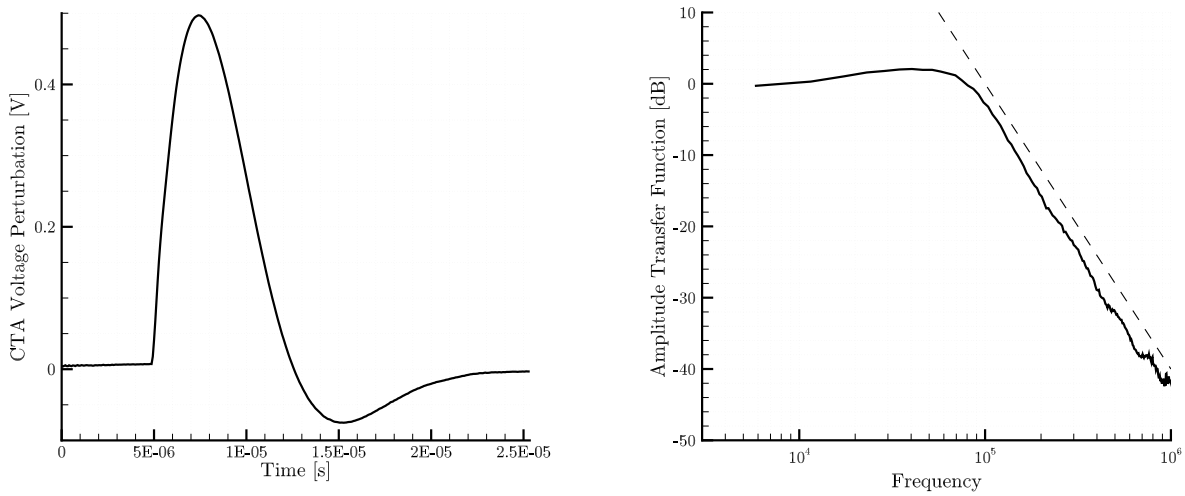


(a) DISA CTA step response in time domain

(b) Fourier transform of DISA CTA step response; Dashed line has -40dB/dec slope

Figure B.7: The analyzing of the DISA CTA transfer function

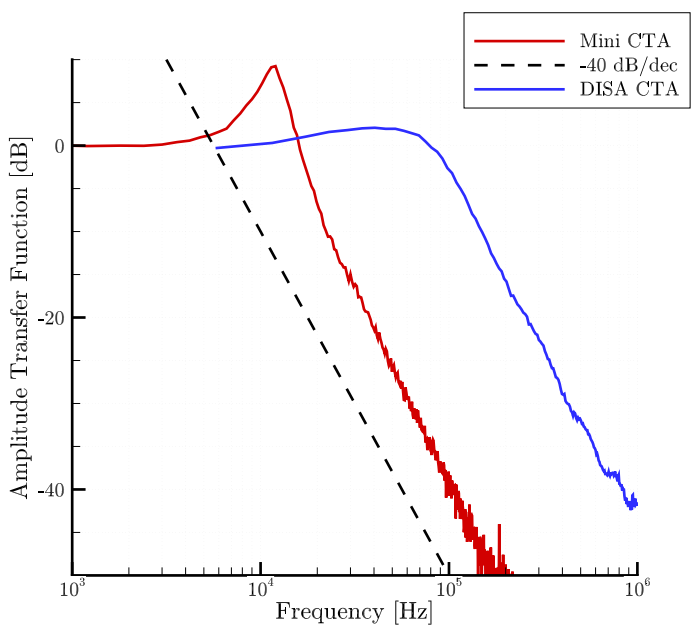


Figure B.8: Comparision of Fourier transform of step response for both types of CTA systems (Figures B.7b and B.4), higher frequency bandwidh and smaller gain for DISA system can be seen here

# Example of complete hardware compensation

Figure C.9 shows the power spectral density of velocity fluctuations at the axis location $x/D = 12$ but for twice the Reynolds number we used in previous paragraph. The non-corrected CVA spectrum is shown together with the spectrum of the signal corrected with the hardware time constant TC1 and the wire time constant $M_{\mathrm{CVA}}$. As we can see it is almost impossible to distinguish one curve from the other. That is because, the software correction induces almost no effect on the CVA signal. This is however just a coincidence due to the fact that at the particular mean velocity for which this measurement has been performed, the time constant $M_{\mathrm{CVA}}$ of the wire was very close to the hardware compensation TC1 of the CVA system, which represents an ideal case that occurs rarely.

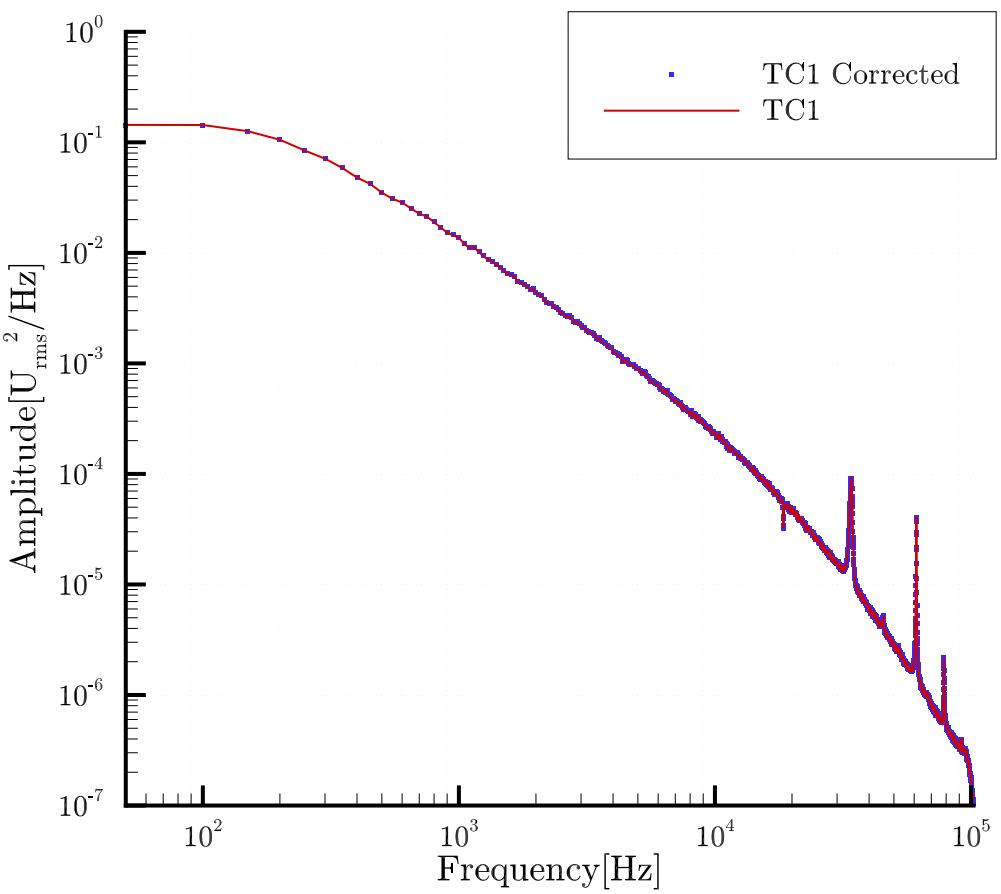


Figure C.9: Power spectra of velocity fluctuations measured on the jet axis at $x/D = 12$ for $Re \simeq 160\ 000$.